

Note: reviewer comment and short comment text is given in blue, while the author response is given in black type underneath.

Response to reviewer comment by Gloria L Manney on “Bifurcation of potential vorticity gradients across the Southern Hemisphere stratospheric polar vortex.”

Jono Conway

We thank Prof. Manney for her helpful and constructive comments. We have made many minor additions and changes to the text to clarify the background and methods. Her comments also led us to extend the method to detect bifurcation to more explicitly exclude periods when the vortex is not well developed enough to analyse. The revised figures 4-12 now further highlight the strong bifurcation in the mid-stratosphere during late winter and spring. We have responded to each of the general and specific comments below.

General Comments:

This paper uses ERA-Interim reanalysis data to describe the climatological bifurcation of potential vorticity gradients in the Antarctic vortex edge region. Overall, the analysis is sound and the paper is well-written. To my knowledge, a detailed description/climatology of the bifurcation of PV gradients in the Antarctic vortex edge region has not been published, and the material will thus be of interest to ACP readers. In its current form, the paper is somewhat lacking in referencing previous work related to vortex edge definitions and mixing barriers, and in explaining the rationale behind the definitions of bifurcation index and other threshold choices used. The introduction, in particular, doesn't provide a clear picture of the relevant background and previous work. Once these issues, and some other specific (minor) points listed below, have been addressed, the paper will be appropriate for publication in ACP.

We have added further background material to the introduction and clarify the choices behind various aspects of the methodology in the text – see specific comments below.

Note 1: Obviously, Zachary Lawrence and I work together. However, we were each notified about the paper separately and each read the paper and wrote up our comments that are posted here independently.

Note 2: I am not suggesting that you cite every one of the numerous Manney et al. papers mentioned in this review; it is inevitable that I am most familiar with those I wrote, and in some cases they may lead you to more appropriate citations; in a couple of cases they are just mentioned as “of interest”.

Specific Comments (in order of appearance in the paper):

Introduction:

Overall, the authors should make clear that much of this discussion (and which parts of it) applies to the Antarctic polar vortex only; many of the statements made are either not applicable to the Arctic vortex, or would need to be qualified (e.g., the discussion of ozone loss and dispersal from the vortex)

to describe the Arctic; this is fine -- the paper focuses on the Antarctic -- but should be said explicitly when there are statements that apply only to the Antarctic. In addition, some statements are rather vague, may not be quite accurate, and/or could use more appropriate citations. Specifically:

Page 1, lines 20--21: "...cold air formed in the polar night..." -- "formed" doesn't seem quite accurate. Changed to "In the Southern Hemisphere, during winter and spring, the barrier isolates the cold stratospheric air that develops during the polar night from warmer mid-latitude air."

- Page 1, line 19: Schoeberl et al (1992) would be a good reference to add to those here; also please use "e.g.," ahead of the reference list in cases like this where there are many papers relevant to the statement. "e.g." added to reference list here and elsewhere. Reference to Schoeberl et al (1992) added.

- Page 1, line 22: Add "e.g.," before or "and references therein" after "(Solomon, 1999)"

'and references therein' added

- Page 1, lines 23--24: Please emphasize that this applies to the Antarctic vortex. "Southern Hemisphere" added before 'polar vortex' on line 23.

- Page 2, lines 1--2: There are many, some earlier, references that could be used here for both statements (I'm sure that is also the case for the statement on line 3, though I am not well-read on such CCM studies). At the very least, "e.g.," or "and references therein" should be used. Some other useful papers to cite (including only ones specifically relevant to the SH) might be:

- Schoeberl et al, 1995 (JGR)

- Lary et al, 1996 (QJ)

- Manney et al, 1999 (JGR), 2005 (JAS), 2005 (GRL)

- Ajtić et al, 2004 (JGR)

Additional references added.

- Page 2, lines 4--18: There are some vortex edge definition methods that are not mentioned here, as well as relevant papers it would be good to cite to briefly discuss other ways the vortex edge or boundary region can be defined besides those you already mention.

The discussion of methods to define the vortex edge(s) has been expanded with many new references.

Also, the statement that "Bodeker et al. (2002) formalised this method" is not accurate: Determining the vortex boundary using the maximum in windspeed x PV gradient is not the same as determining it by the maximum PV gradients but requiring that maximum to be in proximity to the windspeed maximum (see, e.g., the brief discussion in Manney et al., 2007, who implemented and compared the two methods, starting with code provided by Eric Nash for the method described in Nash et al).

The sentence has been changed to:

"The centre of the vortex boundary region is most often defined as the EL of the maximum of the PV gradient times the average wind speed (e.g. Bodeker et al 2002, Manney et al 2007)"

It would also be good to mention some other papers that discuss different ways of defining the vortex edge, especially some of the early papers that use PV gradients (eg, Tronday et al, 1995) and/or use other methods and compare with PV gradient methods (eg, Paparella et al, 1997, JGR, already cited

here but the comparisons are not mentioned; Rummukainen et al, 1994, Ann. Geophys.) Smith and McDonald (2014, JGR) used the “function M ” to look at the strength of the Antarctic vortex and the width (area) of the vortex boundary region. The authors may be interested (though certainly not obliged to cite a paper that will only be available online sometime in the next few days after I’m writing this review) in the vortex edge method in Lawrence and Manney (2017, JGR, in press), which also gives further discussion of various vortex edge definition methods and literature.

These and other references have been added.

- Page 2, line 12: Add “e.g.,” before “Manney and Lawrence, 2016” (I am sure others have done this as well; our two Manney et al (2015) papers are ones where I know this was done). changed to e.g. Waugh and Randel, 1999; Manney and Lawrence, 2016

- Page 2, lines 11--18: May be worth noting that Manney and Lawrence (2016) compared their climatological selection of vortex edge PV values to daily PV gradients, effective diffusivity, the function M, and trace gas gradients. This section has been reworked, so a comment is now not required.

Section 2.1:

It would probably be useful to cite Fujiwara et al. (2017), the overview paper for the SPARC Reanalysis Intercomparison Project, here -- they provide a detailed description of all the commonly used reanalyses. Added in last paragraph of introduction.

While not critical to this paper, it would be interesting to see how the bifurcation changes and where it is present at levels above 850K. I realize that ERA-Interim isentropic level PV data are not provided above 850K, but a few isentropic levels in the upper stratosphere are provided in the CFSR dataset. Could you use that to make a brief comment as to what we might expect at higher altitudes?

We prefer to maintain ERA-interim as the primary dataset, so it does not make sense to present these data here. As noted in other papers (e.g. Manney and Lawrence, 2016), PV gradients are less well defined in the upper stratosphere, so I expect that the method to detect bifurcation may be less valid at these altitudes. The introduction has been amended to emphasize the focus on the mid-stratosphere where the highest rates of ozone depletion occur.

Section 2.2:

Page 3, lines 9--13: The description of this procedure is not clear to me. As I read this, you are using the PV data as distributions from which to find, at each timestep and vertical level, what PV value each of 181 linearly spaced percentile values corresponds to, and then calculating the EL of each of the resulting 181 PV values? Yes – see full explanation below. Since PV as a function of EL is calculated (by whatever method) before the gradients with respect to EL are taken, how could this lead to spurious zero values of PV gradient?

Spurious zero values of PV gradient can occur when equally-spaced PV steps are chosen to calculate EL. Where no PV data falls between the two PV steps, both PV steps are assigned the same EL. In these cases, a spurious zero PV gradient occurs. This is especially the case with CFSR where the data is truncated to a reduced precision. At some levels, the PV data in CFSR has only a few hundred unique values and this creates a significant problem for EL analysis.

Since the fact that there are regions (which vary from day to day) with much weaker and stronger PV gradients means that the resultant PV values at which you find EL will not be uniformly spaced, it appears to me that using the percentile steps might lead to a very non-uniform coordinate mapping

(from lat/lon to EL) and one that changes from day to day and level to level -- could this then have a significant effect on the subsequent numerical derivatives to get the PV gradients? I apologize if I am off the mark with these questions -- if I am, I suspect that also argues for clarifying the description.

In addition to the spurious zero values discussed above, using equally-spaced PV also produces ringing in the CFSR dataset, as the data is truncated to a reduced precision during the analysis using a multiplier that is not always appropriate. To avoid using equally-spaced PV steps, our two options are thus: map the EL of every unique PV value, or find a way to interrogate a useful and reliable subset of PV values. Mapping the EL of every unique PV value is computationally expensive and increases the chances of ringing in the derivatives (as discussed by Nash et al 1996). To be useful, the data can be resampled to regular EL, but this step may introduce its own issues.

We have found the most reliable way to choose a subset of PV values is through percentile steps. Here, we chose to sample 181 percentile values, as this is similar to the number of latitude points per hemisphere in the reanalysis datasets. Each hemisphere is treated separately and for the SH, PV values are multiplied by -1 to ensure a common treatment with NH. To capture the extreme tail of the PV distribution, 8 steps are placed between 99th percentile and maximum value [99, 99.5, 99.75, 99.875, 99.9375, 99.96875, 99.984375, 100th percentiles]. The remaining 173 bins are spread linearly between the minimum (i.e. the most positive PV values in the SH) and 99th percentile. In essence, our method simply takes an a-priori guess at a regular EL spacing (by assuming all grids points have the same area), then chooses PV steps based on that. Other methods assume constant PV spacing to arrive at the same gradients.

We have thought about whether using percentile steps will have an adverse effect on the derived PV gradients, but have not found any evidence that it degrades the quality of the analysis. To illustrate the differences between our method and others, the PV-EL relationship was calculated using percentile steps and equally-spaced steps (denoted linear in Figure 1) for an example time/height (Figure 1; 1 September 2007 at 550K in CFSR). The PV-EL relationship was also calculated at constant steps of 0.1 sPVU or by using all unique PV values, which are then resampled at 0.5 degree EL steps. Figure 1 shows the PV, 1st and 2nd derivatives of PV with respect to EL, PV and EL spacing, and average wind speed for these different methods.

Like any other method, using percentile steps to interrogate the PV-EL relationship will result a different coordinate mapping from day to day and level to level. While the PV spacing when using the percentile method is non-uniform, the EL spacing is close to uniform. Aside from small differences in the precise EL of each step, all methods return very similar PV, wind speed. The gradients returned using percentile steps or all unique PV values show only minor differences and this gives us confidence the results are not sensitive the choice of a particular method. The percentile method has the advantages that PV gradients can be derived directly from the steps used to create the PV-EL mapping, rather requiring the PV-EL relationship to be resampled to reasonable resolution (0.5 degree). Equally-spaced steps show ringing in the first derivative that becomes much worse in the 2nd derivate.

We have updated the description of the method in the manuscript to include more details about the percentile method, along with a comment about the effect on the derivatives obtained.

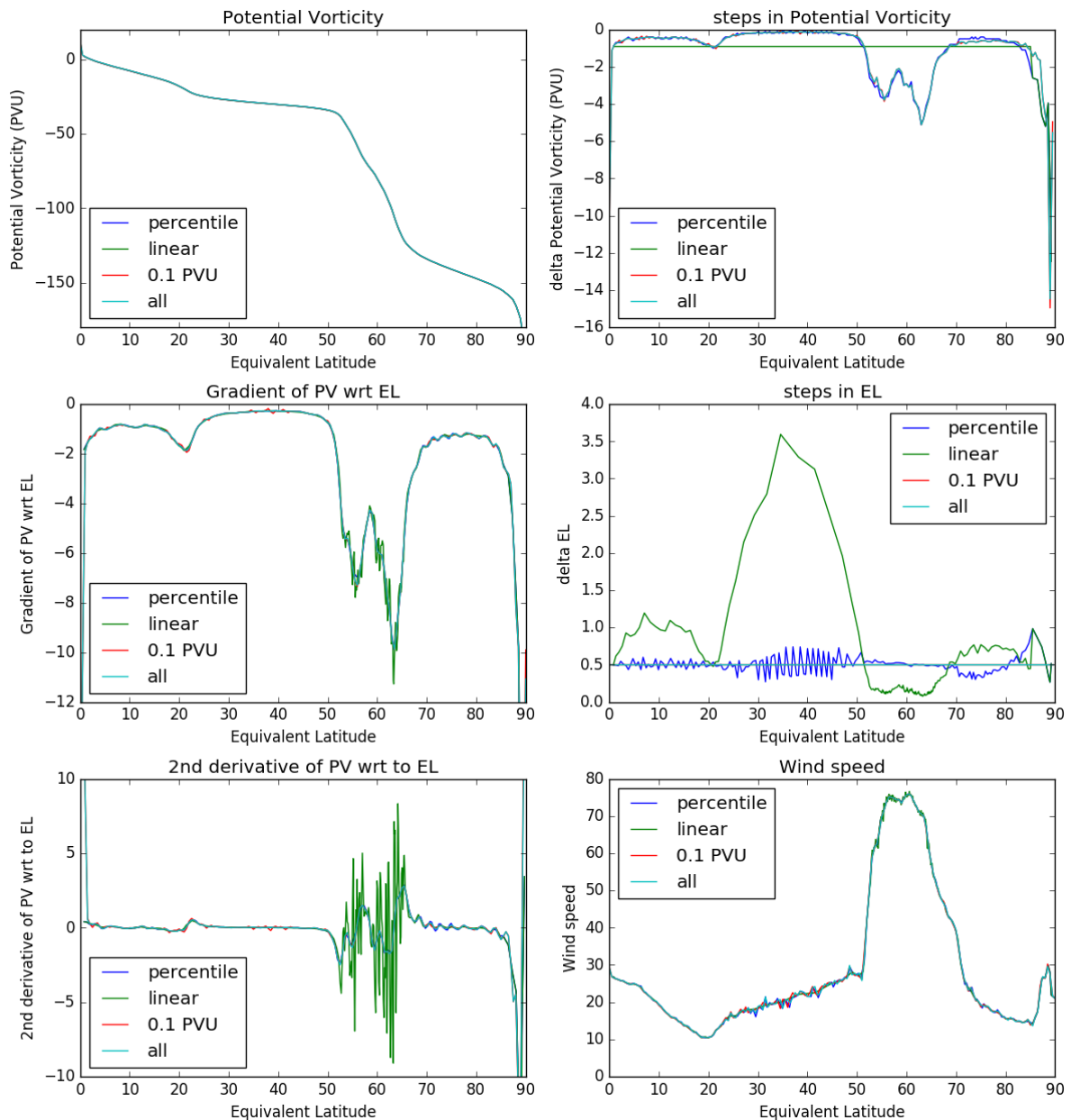


Figure 1. Equivalent latitude calculations using various methods to choose PV steps. All have 181 steps. Percentile = method used in paper; linear = 181 steps evenly-spaced between minimum and maximum PV, 0.1PVU = EL calculated for 0.1 sPVU steps, then distribution resampled to 0.5degree EL steps; all = the same as 0.1PVU but calculated for every unique PV value. This example is for 1 September 2007 at 550K in CFSR.

Page 3, line 16: Is 40deg EL always low enough for the SH polar vortex? This may not be a problem at the middle and lower stratospheric levels you are looking at here, but from the vortex edge diagnostics I've looked at, in the upper stratosphere, especially in the SH, the vortex is often very large, and I frequently found peaks in PV gradients or windspeed x PV gradient that were slightly equatorward of 40deg.

It is likely some peaks are missed at higher levels during mid-winter, but for simplicity a single latitude range was chosen here. An updated Figure 5 shows that peaks close to 40° S are not common. Only at 850K during May through August is it likely for peaks to be missed due to the 40° cut-off; including both primary and secondary peaks, 1.7%, 5.5%, 6.8% and 1.9% of peaks at 850K in these months are

found north of 42.5 degrees, respectively. At other levels much less than 1% of peaks are found close to the 40° cut-off.

Page 3, lines 16--19: Is anything done to eliminate spurious peaks in this primary and secondary peak identification? One of the advantages of using windspeed x PV gradients or constraining PV gradient maxima to be near windspeed maxima is reducing the occurrence of such peaks. Can you say anything about how much of an issue this might be, especially, eg, where you find widely separated peaks and one is near 80 EL where spurious peaks are more common? Also, are any other criteria used (e.g., a minimum windspeed, such as in Nash et al, 1996 and Manney et al, 2007; and/or a minimum PV gradient such as in Manney et al, 2007) to determine when the vortex is well-defined enough to analyze (you do mention a minimum PV gradient criterion in a figure caption later; if this is applied in general, it might be good to move it to this methods description and explain the reasoning behind the choice of value)?

We now introduce a minimum wind speed of 15.2 m/s (Nash et al. 1996) and minimum PV gradient (significantly above average; see methods for calculation) to constrain the detection of primary and secondary peaks, and to determine if the vortex is well developed enough to analyse. Less than 2% of all peaks are found south of 77.5° S at all levels, so spurious peaks near to 80°S are likely not common. The methods section has been updated to reflect this.

Page 3, lines 20 to 28 and Table 1: The rationale behind the choices of combinations of peak ratio and dip fraction for the bifurcation index isn't clear, could you please explain this further? Why does it make sense for the dip fraction to go up as the peak ratio goes up? What did you look at to determine these values (e.g., extensive visual inspection and of what if so, or some other measures)? When you say on lines 24--25 that the dip ratio has more influence on BI, why is that desirable (presumably it is or you wouldn't have made the choices you did)?

The threshold values used for BI were chosen to capture cases with clear bifurcation after extensive visual inspect on PV gradients. For this reason, only peaks with at least 50% the PV gradient of the main peak are considered bifurcated. In the same way, if there is no clear dip between the two peaks, a second maximum is more likely a 'shoulder' on the main peak or noise in the PV gradient. The 5% minimum on the dip fraction was considered large enough to avoid these situations.

The two thresholds increase at the same time so that strong bifurcation requires both a similarly sized secondary peak and a very clear dip between. Without a strong dip, a second peak of similar magnitude more likely represents a wide area of strong PV gradient (or a shoulder on the main peak) rather than a distinct peak in its own right. For this reason, it is desirable for the dip ratio to have a stronger influence on BI – it weeds out the more indistinct peaks.

The threshold values were determined by varying linearly between our chosen extremes for peak ratio (50% and 95%), and the corresponding minimum and maximum peak ratio (5% and 50%). Other combinations of threshold values may also give satisfactory results, but, as the metric is only intended to be a guide, this is not a concern. The BI metric is complemented by the peak ratio and dip fraction, which allow a more nuanced description of a bifurcated profile if desired. The primary reason for the BI metric is to detect the presence of bifurcation and to allow inter-annual variations in bifurcation to be analysed.

Further explanation of these choices is now given in the methods.

How are the various bifurcation diagnostics (BI, as well as peak ratio and dip fraction) affected by changes in EL resolution (e.g., using 91 or 361 percentile steps)? Would such a change significantly affect your results (including the thresholds used to determine BI)?

Changing the resolution to 90 or 360 steps results in very similar patterns of BI, dip fraction and peak ratio, but the frequency of bifurcation is increased (Figure 2). The magnitude of the average peak ratio is not substantially changed with changing resolution, whereas dip fraction increases with increasing resolution. At higher resolutions, the increased dip fraction and more frequency bifurcation increases average BI, but the general pattern is the same. If using a different resolution, the dip-ratio threshold used to define BI may need to be changed, but the story will remain the same. The PV gradient thresholds (mean + 2SD) at 90 and 360 steps are within 1% of the values at 181 steps, so are not sensitive to resolution.

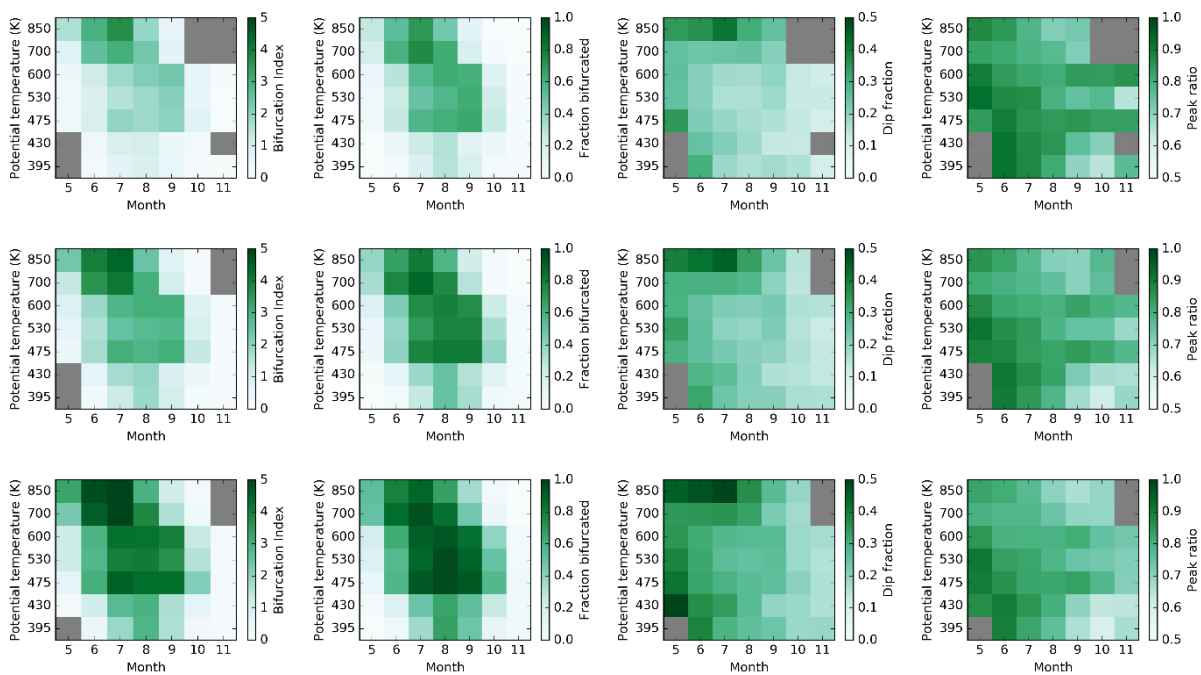


Figure 2. Monthly average BI, fraction of profiles bifurcated, dip fraction and peak ratio (columns from left to right) for 90 (top row) , 181 (middle row) , and 360 (bottom row) percentile steps at selected levels in ERA-Interim [compare to Figure 4 a,e,f].

Figure 1: You might consider using thicker lines and/or bolder colors; while it is OK on a good high-resolution monitor, on many printers or lower resolution monitors, the red line in the lower panel will be barely visible. (A similar comment applies to Figure 9.) Line weight in Figures 1 and 9 has been increased.

Section 3.1:

Page 5, line 9: What is meant by “the inside and outside edges of the region of maximum wind speed”? Since the maximum wind speed is a point (on each isentropic level), the “region” of maximum wind speed is not defined unless you define it, which must be done before you can define the inside and outside of it and whether something is near that. (This occurs again later in the paper as well.)

We have clarified this sentence “While increased climatological PV gradients occur over a broad region, at lower levels these are nearer the poleward edge of the wind speed jet, while at higher levels these are nearer the equatorward edge of the jet”.

Figure 2: Please specify in the caption that these are monthly means (I believe that's true).

Yes, these are monthly means of PV gradients in 0.5 degree bins. Caption amended.

Section 3.2:

Figure 4: It might be helpful to put horizontal lines at the boundaries of what you call "mid-levels", since those are mentioned several times in the text.

We prefer not to add horizontal lines as these would unduly influence how the reader interprets the figure. i.e. we can have suggested a priori what the pattern they should see is.

Also, what is the reasoning behind the choice of the PV gradient threshold?

We previously used a value of 0.45 sPVU to filter the climatology as it was 1.5 times the PV gradient that we had assessed (in other work) as being associated with the boundaries of the vortex edge region. We now introduce a PV gradient threshold into the calculation of the BI metrics and do not use this criterion to filter the climatology. The PV gradient criterion is now defined as the mean + 2*standard deviation of the PV gradient between 5 and 80 degrees at a given level, assessed using profiles from the entire timeseries in all months. We now only filter the monthly average climatology (Figure 4) for periods when bifurcation is present in less than 1% of profiles. We filter the timeseries of monthly averages (Figure 6) when the vortex is not well developed in less than 50% of time periods. The methods section and figure captions have been updated to reflect this.

Section 3.3:

Page 7, line 5 and Figure 5: It isn't at all clear to me that Figure 5 shows the peaks to be "more dispersed in August (which I would take to be "winter" rather than "Spring") than September, if that is what you mean by this statement. If by "earlier in the season" you mean before August, why not show July as well to demonstrate this?

We have clarified this statement to "At 700K and 850K, the locations of primary peaks are spread across a wider range of latitude bins, especially in August."

Section 3.4:

Page 8, line 2: Can you be more specific than "in some years"? How many of the years do you see it in during a significant part of the month?

Average BI > 0.75 in November is only seen in two years (1987 at 475K and 530K, and 2015 at 600K).

Figure 6 shows a sharp change between 430 and 475K in September, which can also be seen in Figure 5 in August and September. Do you have any thoughts on why this might be?

At 430K, secondary peaks are not common (Figure 4b) and are usually closer to the primary peak (Figure 4c) and weaker than at 475K (Figure 4e). There is a shift in the preferred location of secondary peaks – equatorward at 475 and poleward to 430. The mechanism for this change is likely related to the fact that the PV gradients on the inside edge of the vortex boundary at 430K don't strengthen during September as they do between 475K and 600K (See figure 2 and 3). I suspect that the cause of the enhanced PV gradient from 475 to 600K is related to changes in ozone concentrations and temperature, but investigating this would be beyond the scope of this paper.

It would be nice to see August and October in Figure 6 as well as the three months shown, especially since the months that are shown look very different -- what does the transition between these regimes look like? Or at least describe this in the text.

We have added the months August and October to Figure 6 and updated the text to describe the transition between these months. To save space we have also removed July and November, as they are largely redundant (November shows almost no values of BI > 1 and August is very similar to July). The months shown in Figure 6 now align with Figures 5 and 10.

In Figure 6, it is very hard to distinguish the lowest 2-3 values from the zero values that represent times without a sufficiently well-developed vortex -- perhaps you could adjust the color palette and/or find another way to clearly indicate "missing data".

We have introduced a grey colour to denote periods when the vortex is not well developed (more than 50% of profiles within a month do not meet the minimum ws and PV gradient thresholds). We have updated the captions.

Section 4.1:

It would be helpful to have the CFSR plots together with the ERA-Interim ones, to facilitate comparison; this comparison also seems like something that it would be good to show earlier in the paper.

A full formal comparison of ERA-Interim and CFSR is not possible, as each data set has different isentropic levels available for download. We prefer to simply use CFSR to confirm the patterns observed in the ERA-Interim data set are real phenomena, rather than focus on comparing all of the results using two reanalysis data sets. For these reasons, we would prefer to keep the section separate. This same format is also used in recent papers on stratospheric mixing (e.g. Abalos et al, 2016). We clarify our choice to focus on results from the higher-vertical-resolution ERA-Interim data set in the methods section.

Section 4.2:

Figure 9 and discussion: It would be very helpful to show the gradients of relative vorticity, absolute vorticity, and $d(\theta)/dp$ -- it is difficult to judge a change in the gradients from the fields themselves. Also, it would be much more convincing (perhaps the same term is not the dominant factor in all cases? Or not as dominant for all BI values?) if this analysis was done for some sort of climatology or composite of cases with bifurcation rather than a single day in a year that may highlight a particular regime of bifurcation.

We have updated Figure 9 with the gradients of vorticity and static stability with respect to EL, so that the gradients can be directly observed. We have also provided a new figure (new Figure 10) showing height-latitude composites of vorticity and static stability gradients, averaged from the 5 years with the highest BI at mid-levels. The composite analysis reinforces the findings from the case study day, showing BI is associated with elevated vorticity gradients in two locations, along with increased static stability gradients at the inner location.

Page 11, line 3, I'd suggest saying something like "...provide context for recent *reports of* trends in ozone...", since the results of Solomon et al (2016) are controversial. wording changed to 'for recent reports of trends'

Section 4.3:

Page 11, lines 6--9: Not necessarily something to change in the paper, but I just note that such large variations from day to day are fairly common even in cases where there is no bifurcation (e.g., in the NH -- you can see examples of this in pretty much any winter season on some isentropic levels, eg, in the vortex edge PV and area routinely posted on <https://ozonewatch.gsfc.nasa.gov/meteorology/NH.html> -- these are calculated using the method of Nash et al, 1996, but other PV gradient-based methods can suffer from the same problem). This is one reason why a constant climatological value is sometimes preferred over an automated day-to-day calculation for applications where a single value for the vortex edge is needed (e.g., Manney et al., 2007; Manney and Lawrence, 2016; Lawrence and Manney, 2017).

These large day to day variations that we were observing in our analysis of the vortex edge were part of the motivation for this study, and the method presented here partly overcomes this issue. A new figure (new Figure 11) is introduced to demonstrate the difference in the temporal evolution of the vortex edges with and without taking into account bifurcation.

Page 12, lines 6--7 and Figure 10: It would be interesting (and possibly a better demonstration) to compare this with what the inner and outer edges of the vortex boundary region look like when the method of Nash et al. (1996) is used without taking the bifurcation into account.

We have added extra panels to Figure 10 (now Figure 12) to show the position of the inner and outer edges without taking into account bifurcation. Along with the new Figure 11 showing the temporal evolution of the edges in 2007, the added benefit of the BI algorithm is now more clearly shown.

Typographical errors, minor wording suggestions:

Page 1, line 9: suggest changing "reduces" to "decreases" ("reduces" is not commonly used as a verb). Changed to "decreases"

Page 3, line 9: "across the polar vortex" sounds a bit odd, since you are calculating the PV gradients over an EL range that includes both vortex and extra-vortex regions. Perhaps reword this. Changed to "Profiles of PV gradient as a function of EL were calculated..."

Page 3, line 23: When you say "profiles" (this also occurs elsewhere in the paper), do you mean the PV gradient vs EL curves for each time? This may seem a trivial point, but can be confusing to those of us who automatically think "vertical" when they see the word "profile"! Perhaps you could orient those of us who are thinking in a different direction by, the first time you use the terminology, saying something like "profiles of PV gradient as a function of EL". References to this terminology has been added to the first two paragraphs of the section 2.2

Page 6, line 9, "display" should be "displays" (or "wind speed" should be "wind speeds"). Changed to 'display'

Page 6, line 12, suggest "decreases" instead of "reduces" Changed to 'decreases'

Figure 6 caption, should be "Data are", not "Data is" Sentence has been removed from caption

Page 9, line 4, "pause" (implies a time variable) doesn't seem like the right word here. "Pause" changed to "weakening"

Response to short comment by Zachary D. Lawrence on “Bifurcation of potential vorticity gradients across the Southern Hemisphere stratospheric polar vortex.”

Jono Conway

We thank Zachary Lawrence for his thoughtful and positive comments on our manuscript. Below we provide responses to his specific comments:

Comments and Questions

1. The introduction is rather short. While it is nice to have it be concise, the introduction in its present form does not discuss any previous examinations of the SH vortex boundary region. I do not know of any papers that show or mention the bifurcation of PV gradients, but there are many studies (some of which are already cited in the paper) that have discussed and shown that the SH vortex boundary region is often quite wide, especially relative to the NH vortex. Many of these studies have used more complicated diagnostics than PV gradients (e.g., effective diffusivity) to show this, so mentioning and briefly discussing such papers would reinforce the following statement in the intro “Because of the minimal computational requirements, the PV gradient is an attractive method to define the vortex boundary region.” Some potential relevant references are already cited in the paper; for example, see figures and related discussion on: Figures 3 – 5 in Paparella (1997) show trajectories of balloons trapped inside the SH polar vortex core and polar vortex boundary; Figures 1 & 2 in Lee et al. (2001) show the width of the vortex boundary region in effective diffusivity during 1996; and plates 1 – 4 in Haynes and Shuckburgh (2000) show monthly means of effective diffusivity that can allow comparison of the widths of the Arctic vs Antarctic vortex boundaries. Other more recent studies that may or may not be relevant to look at include (but certainly are not limited to): de la Cámara et al., JAS, 2012; Abalos et al., QJRMS, 2016; and Curbelo et al., NPG, 2017.

We now make a larger discussion of the various methods to detect the vortex boundary in the introduction.

2. Tied to 1, the results shown in the current paper could be made more impactful in both the introduction and conclusions by being more clear about the “magnitude” of what is shown. In my opinion, the paper sells itself a bit short. More specifically, I mean that many previous studies (including some of the ones discussed in comment #1) only show results relevant for a single dataset for one to a few winters; this paper shows results relevant for two reanalyses for years from 1979 to roughly the present. I think that is worthy of being highlighted as one of the strong points of the paper.

We have highlighted these points in the conclusions.

3. This is very minor, but in section 2.1, the years used for ERA-Interim and CFSR should be listed.

Dates for each reanalysis have been added.

4. Figure 1 and Table 1 are helpful, but it would be nice if a new figure was included showing EqL profiles of PV gradients for different values of the BI. For example, a 2 x 3 figure with panels showing (along with dates, isentropic levels, peak ratios, and dip fractions listed) representative cases with BI = 0, 2, 4, 6, 8, and 10. I think this would give the reader a better sense of the connection between BI and the geometry of the PV gradient profiles, as well as enhance understanding and the significance of the other figures in the paper.

During the preparation of the manuscript we considered adding a figure like this, but opted not to for brevity. We describe the range of bifurcated profiles in paragraph 3 of Section 2.2.

5. In Section 3.1 and Figure 2, is it really accurate to say that there are two regions of enhanced PV gradients? Since there is no clear dip, it looks as if there is only one broad region of enhanced gradients in all cases, even though the location of the climatological maximum gradients moves “equatorward” with height in August & September. This pattern seems to be clearly formed from averaging many cases with bifurcated PV gradients having peaks in different EqL locations, which would strengthen the idea that the PV gradient bifurcation needs to be examined on a year-to-year basis to really see and understand it (i.e., as is shown in Figure 3).

Agreed, the two regions are most clearly identified in the individual years, whereas the climatological gradients smear the gradients. We have reworded this sentence:

“In August and September, PV gradients intensify in concert with the region of strong wind speed becoming predominately confined to latitudes poleward of -50° . While increased climatological PV gradients occur over a broad region, at lower levels these are nearer the poleward edge of the jet, while at higher levels these are nearer the equatorward edge of the wind speed jet (Figure 2 c,d).”

6. In Figure 3, I would be curious to see whether the bifurcated structure also shows up in “regular” zonal means of meridional PV gradients (i.e., with respect to “regular” latitude), since the SH flow and PV distributions are usually relatively close to zonally symmetric. If the bifurcated structure also exists in the zonal mean picture, this could be an interesting result with further implications (e.g., for wave guiding/propagation).

Agreed, this would be an interesting analysis, but it is beyond the scope of the paper so do not plan to make these analyses here.

7. The comparison with CFSR in section 4.1 is so short that it almost seems unnecessary. First of all, why not show all the same panels for CFSR in Figures 7 and 8 as those in Figures 4 and 5? And since section 4.1 is so short, why not fold the CFSR results from Figures 7 and 8 into Figures 4 and 5 (and maybe even Figure 6) and discuss the comparisons in sections 3.3 and 3.4 directly? Figures 4 and 5 would obviously increase in size (and more labels would be necessary), but there would be an advantage to having the results from the two reanalyses side-by-side for easier comparison, and less figures overall. This would also reinforce one of the strengths of the paper (see my comment #2).

Because of the better vertical resolution of the ERA-Interim data set, we prefer to restrict the main results to ERA-Interim and keep the comparison with CFSR separate. The comparison needed, but simply there to show that the patterns we observe are real phenomena, and not the product of the methods used to calculate them in a particular reanalysis. Because the ERA-Interim and CFSR data sets are produced on different potential temperature levels, a formal quantitative comparison is not possible. We have added additional panels to Figures 7 and 8 to present further results for CFSR

8. Figure 9 and its discussion in Section 4.2 would be a bit more useful/significant if Figure 9 showed composites of some form, so that readers would know the discussion is more broadly relevant than to a single day of data. I do realize, however, that this may not be easy or possible to do since the locations of peaks in PV gradients (and hence the geometry of the PV and relative/absolute vorticity profiles) will vary from day to day – but it is something that might be worth a try.

We have also provided a new figure (new Figure 10) showing height-latitude composites of vorticity and static stability gradients, averaged from the 5 years with the highest BI at mid-levels. When PV gradients are bifurcated at mid-levels during August and September (Figure 10 d-i), there are distinct

locations for the primary and secondary peaks and the composite analysis reveals some useful patterns. The composite analysis reinforces the findings from the case study day, showing BI is associated with elevated vorticity gradients in two locations, along with increased static stability gradients at the inner location.

9. Also in Figure 9 – how were the fields of relative/absolute vorticity obtained? Were they derived from the potential vorticity and temperature fields, or the wind components, or were they downloaded?

Relative vorticity was downloaded from the ECMWF online archive. Absolute vorticity was calculated from relative vorticity and latitude at each grid point. The lapse rate of potential temperature was back-calculated from PV, relative vorticity and latitude at each grid point and the equation for Ertel PV. These details have been added to the text.

10. The following is just an idea I had, but something the authors might consider: The current organization of the paper is fine, but since the paper is largely focused on presenting the methods and diagnostics, there is an alternative organization I see that might flow better for readers (and would only require minimal work). Arguably the bifurcation detection methods and diagnostics are part of the results of the paper. Thus, section 2 could be changed to a “Data and Background” section wherein section 2.1 would remain the same, section 2.2 would discuss how the EqL profiles of PV and PV gradients are obtained, but a new section 2.3 would be inserted (the background) that included Figures 2 and 3 (which would become Figures 1 and 2) and their discussion. The BI panel in Figure 3 would have to be changed to something like “average peak separation in degrees EqL” since BI would not be introduced yet. Then in section 3, the description of the bifurcation detection and diagnostics (and the current Figure 1) would be included in section 3.1 with a title like “PV gradient bifurcation detection and diagnostics.” This organization would lead readers from the climatologies (which smear out the bifurcated gradients), to a single SH winter that illustrates the phenomenon, to the detection methods and bifurcation diagnostics, and finally to the results/figures that directly show the BI and other diagnostics (which, with this organization, would have just been defined). Again, this is just an idea; the authors should feel free to flatly reject it!

Thanks for the reorganisation suggestion – but we’ve opted to keep our original organisation.

Response to reviewer comment by Petr Šácha on “Bifurcation of potential vorticity gradients across the Southern Hemisphere stratospheric polar vortex.”

Jono Conway

I think that it is absolutely vital for your study to reconsider your results with respect to the recently published work by Serra et al. (2017). Their geodesic method identifies a materially optimal vortex boundary. More to that, Serra et al. (2017) show also a comparison of their method with a "Nash" vortex boundary. To cite some of their conclusions: "Nash method is frame dependent and nonmaterial, hence a priori unsuitable for a self-consistent detection of coherent transport barriers." "Given its Eulerian (nonmaterial) nature, the Nash edge evolves discontinuously, with visible jumps in position and shape over time."

My personal opinion would be that your analysis of PV gradients may be untouched, but the relationship to mixing barriers needs to tackle these new findings.

We thank Petr Šácha for bringing to our attention the recent paper published by Serra et al 2017 'Uncovering the Edge of the Polar Vortex'. This paper presents a method for detecting the area of the relatively undisturbed airmass within the polar vortex using a Lagrangian framework and thresholds in deformation coefficients along the boundaries. They provide a brief comparison of their kinematic boundary to that defined using the method of Nash et al (1997) for the Northern Hemisphere polar vortex for a short period 2013.

As mentioned in the comment and the response by Gloria Manney, the findings of Serra et al. 2017 are mostly relevant to a definition of the the vortex edge, and not to the main result of our manuscript (which concerns PV gradients). We agree there is a need to thoroughly review the definitions of the vortex boundary, formally compare the various methods to detect these boundaries and quantitatively compare the transport and mixing properties associated with the vortex in the Southern Hemisphere. But this task is well beyond the scope of the current manuscript. We have included Serra et al. (2017) in list of Lagrangian metrics used to identify the vortex edge in the introduction.

Bifurcation of potential vorticity gradients across the Southern Hemisphere stratospheric polar vortex.

Jonathan Conway¹, Greg Bodeker¹, and Chris Cameron¹

¹Bodeker Scientific, 42 Russell Street, Alexandra, 9320, New Zealand

Correspondence to: J.P. Conway (jono@bodekerscientific.com)

Abstract. The winter-time stratospheric westerly winds circling the Antarctic continent, also known as the Southern Hemisphere polar vortex, create a barrier to mixing of air between middle and high latitudes. This dynamical isolation has important consequences for export of ozone-depleted air from the Antarctic stratosphere to lower latitudes. The prevailing view of this dynamical barrier has been an annulus comprising steep gradients of potential vorticity (PV) that create a single semi-permeable barrier to mixing. Analyses presented here show that this barrier often displays a bifurcated structure where a doubled-walled barrier exists. The bifurcated structure manifests as enhanced gradients of PV at two distinct latitudes - usually on the inside and outside flanks of the region of highest wind speed. Metrics that quantify the bifurcated nature of the vortex have been developed and their variation in space and time has been analysed. At most isentropic levels between [370K-395K](#) and 850K, bifurcation is strongest in [winter and reduces mid-winter and decreases](#) dramatically during spring. From August onwards a distinct structure emerges, where elevated bifurcation remains between 475K and 600K, and a mostly single walled barrier occurs at other levels. While bifurcation at a given level evolves from month to month, and does not always persist through a season, inter-annual variations in the strength of bifurcation display coherence across multiple levels in any given month. Accounting for bifurcation allows the region of reduced mixing to be better characterized. These results suggest that improved understanding of cross-vortex mixing requires consideration of the polar vortex not as a single mixing barrier, but as a barrier with internal structure that is likely to manifest as more complex gradients in trace gas concentrations across the vortex barrier region.

1 Introduction

The polar vortex is the defining dynamical feature of the stratosphere during winter and early spring. The steep gradients in trace gas concentrations and in dynamical tracers such as potential vorticity (PV) across the vortex boundary region indicate a dynamical barrier to the mixing of air between the mid-latitude and the high latitude stratosphere ([Hoskins et al., 1985](#), e.g. [Schoeberl et al., 1992](#); [Hoskins et al., 1985](#); Plumb and Ko, 1992). In the Southern Hemisphere, during winter and spring, the barrier isolates [the](#) cold stratospheric air [formed in that develops during](#) the polar night from warmer mid-latitude air. The polar stratospheric clouds that form in this region provide the conditions needed for the heterogenous chemical reactions that create the halogen radicals that go on to deplete ozone ([Solomon, 1999](#))([Solomon, 1999 and references therein](#)). In springtime, the barrier prevents ozone depleted air within the [Southern Hemisphere](#) polar vortex from mixing with ozone rich air that accumu-

lates in the downward branch of the Brewer-Dobson circulation equatorward of the vortex. By defining the location of the polar vortex in equivalent latitude (EL) coordinates (Butchart and Remsburg, 1986), the temporal evolution of the size and strength of this dynamical containment of ozone depletion can be assessed (~~Bodeker et al., 2002~~) (e.g. [Bodeker et al., 2002](#)) and periodic mixing of air masses into and out of the vortex can be identified (~~Manney and Lawrence, 2016~~) (e.g. [Schoeberl and Newman, 1995](#);
5 [Paparella et al., 1997](#); [Ajtić et al., 2004](#), [Manney et al., 2005](#)). Providing a quantitative description of the vortex barrier also allows the representation of the polar vortex in coupled chemistry-climate models to be evaluated (~~Struthers et al., 2009~~) (e.g. [Struthers et al., 2009](#)).

The centre of the vortex boundary region is most often defined as ~~the location~~ (i) [the EL of the maximum gradient of PV with respect to EL](#) (herein referred to as PV gradient), with the caveat that the true peak is also located in the region of the maximum
10 westerly jet (~~Nash et al., 1996~~). ~~Bodeker et al. (2002) formalised this method by defining meridional impermeability as the product~~ (e.g. [Nash et al., 1996](#)), or (ii) [the EL of the maximum of the PV gradient](#) ~~and times~~ the average wind speed ~~in the same EL coordinates~~ (e.g. [Bodeker et al., 2002](#); [Manney et al., 2007](#)). ~~The inner and outer edges of the vortex boundary region can be assessed using the change in the curvature of the vortex definition function (PV gradient or PV gradient times wind speed).~~ Because there is a one-to-one correspondence between PV values and EL (see Figure 1a of [Nash et al., 1996](#)), ~~identifying the EL of the centre of the vortex boundary region allows the PV value corresponding to the centre of the~~ [the PV values corresponding](#)
15 vortex boundary region ~~to be ascertained. This allows polar vortex tracking algorithms (e.g. Manney and Lawrence, 2016) can be used~~ to map the size and location of the vortex in latitude-longitude coordinates. ~~Because of the temporal variability in the vortex, these methods sometimes rely on climatological PV gradients to define PV values that correspond to the centre of the vortex boundary region (Manney and Lawrence, 2016). The inner and outer edges of the vortex boundary region can be defined using the second derivative of PV with respect to EL. These edges can then be combined with trajectory model calculations to quantify transport into and out of the vortex boundary region (Paparella et al., 1997). The Methods to map the vortex in two dimensions often use climatological PV values corresponding vortex boundary (e.g. Waugh and Randel, 1999; Manney and Lawrence, 2016) because PV gradients exhibit large temporal variability and because the vortex is sometimes poorly defined. Analyses using climatological PV values can represent inter-annual variations in vortex attributes well, but~~
20 ~~may not represent the size of the Southern Hemisphere polar vortex well during the spring, as the PV value associated with the strongest PV gradients changes (e.g. Waugh and Randel, 1999). Besides diagnostics using PV gradients, the vortex boundary can also be defined by calculating the gradient of trace gas concentrations in the same EL coordinates as PV, through using maximum wind speed in longitudinal bins (e.g. Rummukainen et al., 1994), maximum kinetic energy (e.g. Paparella et al., 1997), concentrations of long-lived trace gases (e.g. McDonald and Smith, 2013). Lagrangian metrics such as~~
30 ~~the Lyapunov exponents (Garny et al., 2007), or Lyapunov exponents or Function M (e.g. Garny et al., 2007; Smith and McDonald, 2014; Serra et al., 2017), the complexity of tracer gradients through effective diffusivity (Haynes and Shuckburgh, 2000) (e.g. Haynes and Shuckburgh or a combination of different metrics (e.g. Manney and Lawrence, 2016; Lawrence and Manney, 2018).~~ Because of the minimal computational requirements ~~and its basis as a dynamical constraint on mixing~~, the PV gradient is an attractive method to define the vortex boundary region.

The increased resolution of recent reanalyses ([Fujiwara et al., 2017](#)) now allows us to resolve the structure of PV gradients in EL coordinates around the polar vortex in much finer detail than was available when the Nash et al. (1996) definition was proposed. This paper investigates PV gradients during late winter and spring over the altitude range where the highest rates of Southern Hemisphere ozone depletion occur (mid-stratosphere). The aim of this paper is to characterise, in detail, [PV gradients across](#) the Southern Hemisphere polar vortex dynamical barrier [within the mid-stratosphere](#), including the vertical and latitudinal structure, seasonal evolution and internal structure of the vortex boundary region.

2 Methods

2.1 Data sets

The primary data set used in this paper is the ERA-Interim reanalysis (Dee et al., 2011) produced by the European Centre for Medium-Range Weather Forecasting (ECMWF). This reanalysis uses a 4D variational assimilation system to combine observed climate variables in a dynamically consistent fashion. Zonal and meridional wind speed, and Ertel potential vorticity (PV) data were downloaded on nine potential temperature (Θ) levels (350K, 370K, 395K, 430K, 475K, 530K, 600K, 700K, 850K) from the ECWFMF online archive on a regular latitude-longitude grid with a resolution of 0.75° in both dimensions [at a 6-hourly timestep for the period 1979-2016](#). To ensure that features observed in ERA-Interim are not unique to a single reanalysis, data from the National Centers for Environmental Prediction (NCEP) Climate Forecast System Reanalysis (CFSR; Saha et al., 2010) and its continuation, the Climate Forecast System version 2 (CFSv2; Saha et al., 2014), were also analysed. For simplicity, the combination of these two NCEP data sets are referred to here as CFSR, though we note slight changes in model parameterizations between CFSR and CFSv2 (see Saha et al., 2014). Zonal and meridional wind speed, temperature and Ertel PV fields from CFSR were downloaded on six Θ levels (350K, 400K, 450K, 550K, 650K, 850K) on a 0.5° regular latitude-longitude grid [at a 6-hourly timestep for the period 1979-2016. The ERA-Interim reanalysis has a higher vertical resolution than CFSR in the lower and middle stratosphere, so we focus on results from this reanalysis, rather than present all the results using both reanalyses.](#)

To facilitate comparison of PV gradients on different Θ levels, PV was scaled to have a similar range of values throughout the stratosphere using the scaling factor $\Theta/\Theta_0^{-9/2}$ (Lait, 1994), with a reference level (Θ_0) of 350K. For ease, PV is also presented here in PVU ($10^6 \text{ Km}^2 \text{ kg}^{-1} \text{ s}^{-1}$), referred to as sPVU when PV has been scaled according to Lait (1994). [Note this scaling is similar to that of Dunkerton and Delisi \(1986\), used in other studies \(e.g. Manney and Lawrence, 2016\), but that the scaled values are of a different magnitude.](#)

2.2 Detection of bifurcated PV gradient

~~PV gradients across the polar vortex~~ [Profiles of PV gradient as a function of EL](#) were calculated by first determining the one-to-one relationship between PV and EL for each time step [and vertical level](#) in the reanalyses ~~(6 hourly)~~. ~~EL is the true latitude that would enclose the same area as that enclosed by a given PV contour (Butchart and Remsberg, 1986)~~. Here, EL was

~~determined~~calculated for 181 PV values that were determined using percentile steps between the maximum and minimum PV at each time step. Each hemisphere is treated separately and in the Southern Hemisphere, PV values are multiplied by -1 to ensure a common treatment with Northern Hemisphere. Of the 181 steps, 174 are linearly spaced between the minimum and 99th percentile, while 7 increasingly small percentile steps capture the extreme tail of the PV distribution (percentiles: 99.5, 5 using percentile steps 99.75, 99.875, 99.9375, 99.96875, 99.984375 and 100). Percentile steps were used to avoid spurious zero values of PV gradient that occur when PV gradient values that can occur when using equally-spaced PV steps: when no PV data falls between two successive equally-spaced PV steps, both PV steps are assigned the same EL and a spurious zero PV gradient value occurs. As well as reducing spurious zero-gradient values, percentile steps reduce ringing in the derivative of PV gradient that can occur when using equally-spaced PV steps. Like any other method, using percentile steps to interrogate the PV-EL relationship results a different coordinate mapping from day to day and level to level. While the PV spacing is non-uniform, the resulting EL spacing is close to uniform as we take an a-priori guess at a regular EL spacing (by assuming all grids points have the same area), rather than choosing equally-spaced PV values to arrive at the same gradients. We have checked that the PV gradients are not dependent on our choice of the percentile method (not shown).

To characterise the bifurcation of the vortex barrier, an algorithm was developed to detect secondary peaks in profiles of PV gradient as a function of EL as follows (see also Figure 1a):

- The primary peak is identified by the largest value of PV gradient between -40° and -80° equivalent latitude.
- A secondary peak is identified as a local maximum in PV gradient that exceeds a fraction (peak ratio) of the primary peak, that is located a sufficient distance (separation) from the primary peak. In addition, the PV gradient between the two peaks must decrease by a fraction (dip fraction) of the secondary peak in PV gradient.

In order to capture peaks only at times and locations where the vortex is well developed enough to analyse, we introduce a minimum zonal wind speed of +15.2 m/s (Nash et al., 1996) and a requirement for the PV gradient to be significantly above average (c.f. Manney and Lawrence, 2016), for both primary peak and secondary peaks. The minimum PV gradient (sPVU) varies between levels [395K=0.331, 430K=0.375, 475K=0.466, 530K=0.534, 600K=0.552, 700K=0.558, 850K=0.480] and is defined as the mean + 2 x standard deviation of the PV gradient using data between -5° and -80° EL for all time periods from 1979-2016.

A bifurcation index (BI) is derived using combinations of peak ratio and dip fraction that are increasingly restrictive as shown in Table 1. Single peaks are denoted as BI = 0 when the peak ratio is less than 0.5 or the dip fraction is less than 0.05. ~~Two choices of separation (2° and 5°) were analysed for all results. Apart from the expected increase in the fraction of bifurcated profiles detected and smaller average BI for 2° separation, the results do not change substantially. The more restrictive~~ The threshold values used for determining BI were chosen to capture clearly bifurcated profiles after extensive visual inspect on PV gradients - hence only peaks with at least half the PV gradient of the main peak are considered bifurcated. In the same way, more than a 5° separation is used hereafter to highlight the structure of moderate to strong bifurcation. The dip fraction was found to have more influence in determining % dip is required between two peaks, to avoid misclassifying a shoulder on the main peak or noise in the PV gradient as a second peak. The two thresholds increase at the same time so that strong

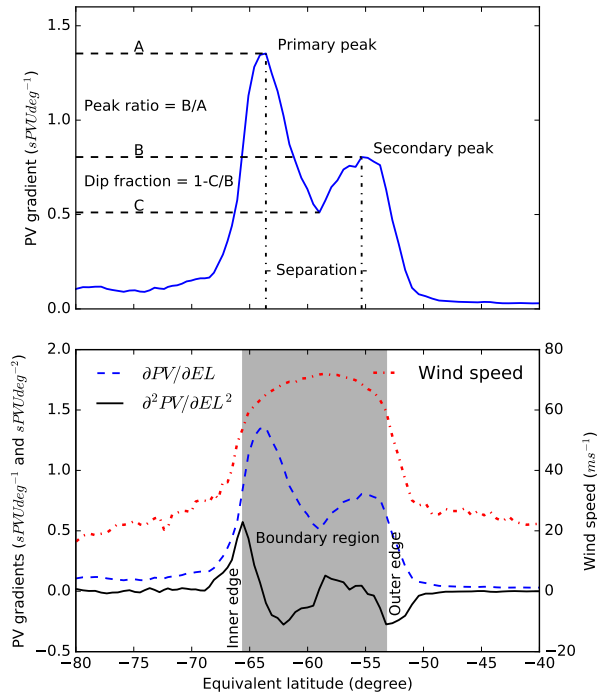


Figure 1. Example of (a) the calculation of the peak ratio, dip fraction and separation from a meridional profile of PV gradient ($\partial PV/\partial EL$) and (b) the calculation of inner and outer edges of the vortex boundary region from $\partial^2 PV/\partial EL^2$ ($sPVUdeg^{-2}$), with wind speed (ms^{-1}) and $\partial PV/\partial EL$ ($sPVUdeg^{-1}$) also shown for reference. This example is a profile at 530K on 1 September 2007 from ERA-Interim.

bifurcation requires both a similarly sized secondary peak and a very clear dip between. Without a strong dip, a second peak of similar magnitude more likely represents a wide area of strong PV gradient rather than a distinct peak in its own right. For this reason, the dip fraction has a stronger influence on BI than peak ratio. Large peak ratios occur in profiles assessed with small to moderate BI, whereas the dip fraction closely follows the threshold values used to define BI, whereas large peak ratios occur in profiles assessed with both small and moderate BI (not shown). Thus, profiles assessed with small to moderate BI can range from two closely matched peaks with only a small interstitial dip, to a much smaller secondary peak on the shoulder of the primary peak. Two choices of separation (2? and 5?) were analysed for all results. Apart from the expected increase in the fraction of bifurcated profiles detected and smaller average BI for 2? separation, the results do not change substantially. The more restrictive 5? separation is used hereafter to highlight the structure of moderate to strong bifurcation.

The inner and outer edges of the vortex boundary region were calculated following Nash (1996); the inner and outer edges are evaluated as the local maximum and minimum in the second derivative of PV with respect to EL around the location of the peak in PV gradient, respectively (Figure 1b). Note that the sign of the second derivative is opposite to the description in Nash et al. (1996) because of the negative sign convention for EL in the Southern Hemisphere. For bifurcated profiles, we nuance

Table 1. Threshold values of peak ratio and dip fraction used to define the bifurcation index (BI).

Bifurcation Index	Peak Ratio		Dip Fraction
0	< 0.5	or	< 0.05
1	≥ 0.5	and	≥ 0.05
2	≥ 0.55	and	≥ 0.1
3	≥ 0.6	and	≥ 0.15
4	≥ 0.65	and	≥ 0.2
5	≥ 0.7	and	≥ 0.25
6	≥ 0.75	and	≥ 0.3
7	≥ 0.8	and	≥ 0.35
8	≥ 0.85	and	≥ 0.4
9	≥ 0.9	and	≥ 0.45
10	≥ 0.95	and	≥ 0.5

the Nash et al. (1996) definition by evaluating the inner edge around the poleward peak and outer edge around the equatorward peak.

3 Results

3.1 Structure of meridional PV gradients in ERA-Interim

5 Figure 2 shows the climatological mean (1979-2016) structure of PV gradients across the polar vortex during the winter and spring. Large PV gradients generally align with the region of enhanced wind speed, which is largest at high levels during mid-winter. In August and September, PV gradients intensify in concert with the region of strong wind speed becoming predominantly confined to latitudes poleward of -50° . ~~At mid-levels, between 475K and 600K, two regions of enhanced PV gradient are visible, aligned with the inside and outside edges of the region of maximum wind speed~~ While increased climatological PV
10 gradients occur over a broad region, at lower levels these are nearer the poleward edge of the wind speed jet, while at higher levels these are nearer the equatorward edge of the jet (Figure 2c, d). As spring progresses, the vortex barrier region narrows and the end of October only a ~~single narrow~~ region of elevated PV gradients remains.

Considering individual years, the bifurcation of PV gradients with respect to EL becomes more apparent. The characteristic evolution of the bifurcated structure is clearly illustrated during the year 2007 (Figure 3). The PV gradient displays two distinct
15 peaks - one aligned with the ~~inside and outside flanks of the region of maximum wind speed, while transition to steep wind speed gradients on the equatorward side of the jet and a second peak in a similar position on the poleward flank of the jet.~~ Between these peaks, near the region at the ~~wind speed maximum has maximum wind speed at mid-levels, are~~ notably reduced PV gradients. The bifurcation of PV gradients is not mirrored in the wind speed, which ~~display displays~~ only a single broad

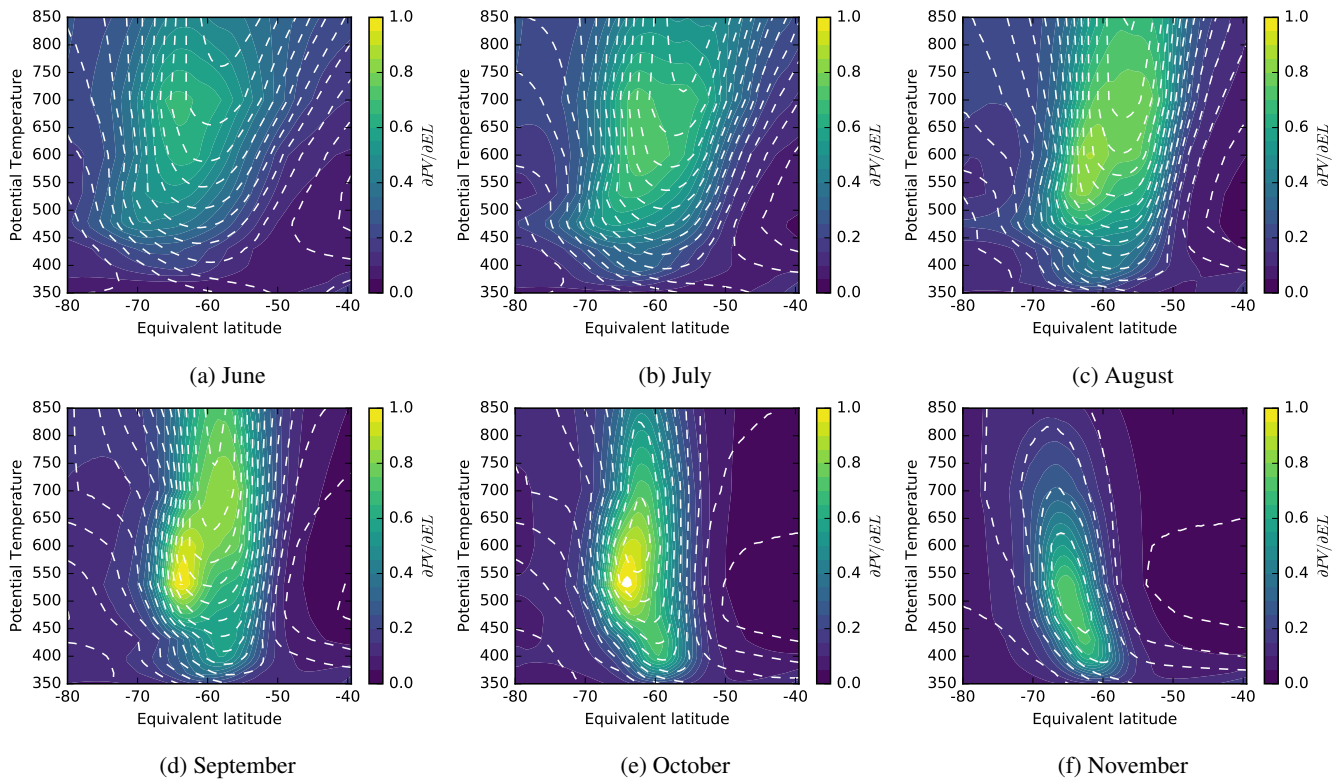


Figure 2. Average Monthly mean PV gradient (colours; $sPVUdeg^{-1}$) and wind speed (dashed lines; in 10 ms^{-1} steps) in 0.5° bins at ERA-Interim levels between 350K and 850K, for selected months, 1979-2016.

region of maximum wind speed. Moderate to high BI ~~is established at most levels during winter~~, but moderate BI remains ~~only at mid-levels as PV gradients intensify during spring~~ occurs at mid-levels during winter and intensifies at 475K during September (Figure 3c).

3.2 Bifurcation metrics

- 5 Generally, ~~early and mid-winter show high average BI, with BI weakening from August onwards~~ the magnitude of BI and the frequency of bifurcation increases during the winter to peak in July or August (Figure 4a), ~~then decreases during spring~~. Low BI during October and November indicates that the vortex barrier has only a single peak, or is weakly bifurcated. ~~The exception is~~ At mid-levels (475K to 600K), ~~where~~ elevated BI remains through September, and, to a lesser extent, October. During September, the barrier is more often than not bifurcated at these levels (Figure 4b). At all levels, the average separation
- 10 between primary and secondary peaks ~~reduces~~ decreases through the season from around 10° in June to around 5° in October (Figure 4c). During the winter, there is only a slight tendency for secondary peaks to occur equatorward of primary peaks (Figure 4d). ~~As spring progresses~~ From August onwards a more defined spatial structure develops; at mid-levels the secondary

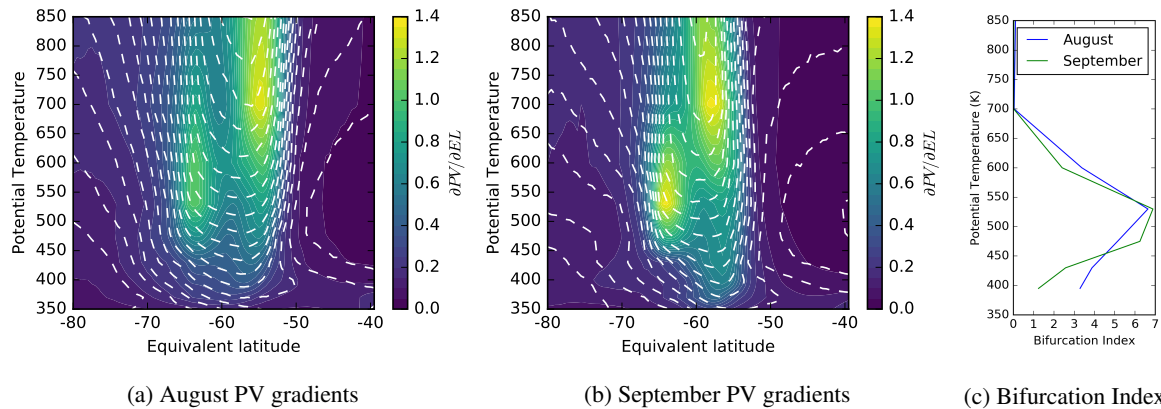


Figure 3. Average-Monthly mean PV gradient (colours; $sPVUdeg^{-1}$) and wind speed (dashed lines; in 10 ms^{-1} steps) in 0.5° bins during (a) August and (b) September 2007 at ERA-Interim levels between 350K and 850K. Also shown is (c) mean BI at each level for each month.

peak is most often equatorward of the primary peak, ~~while at~~. At other levels the secondary peak is more often poleward of the primary peak. ~~The small BI at low and high levels (Figure 4a) indicate that~~, though secondary peaks at these levels are ~~either weaker and~~ not as common ~~as those or strong as~~ at mid-levels. Maximum-During September, maximum values of peak ratio occur ~~during September~~ at 475K and 600K, indicating that two peaks with similar magnitude occur frequently at these levels (Figure 4e). The general decline in dip fraction over the season mirrors the decline in BI, showing its strong influence on BI (Figure 4f).

3.3 Location of primary and secondary peaks

The locations of primary and secondary peaks in PV gradient have a well-defined structure during late winter and early spring. At mid-levels (475K to 600K), peaks in PV gradient occur in two preferred locations centred around -63° and -55° (Figure 5), with primary peaks being most often in the poleward location, and secondary peaks in the equatorward location. ~~Earlier in the season~~ At 700K and 850K, the locations of primary peaks are ~~more dispersed, especially at higher levels (700K and 850K)~~ spread across a wider range of latitude bins, especially in August. At lower levels (370K - 395K to 430K), primary peaks are more tightly clustered around -60° and secondary peaks tend to be to poleward of primary peaks.

3.4 Inter-annual variability in bifurcation

15 Large inter-annual variations in BI display some coherence across multiple levels (Figure 6). For example, during July-August, when bifurcation is common, anomalously low BI occurs simultaneously over multiple levels in a given year (e.g. 1992, 2008, 1996, 2005). During September, vertically coherent inter-annual variations in BI occur at mid-levels, with anomalies in BI that extend through multiple levels and weak BI above and below. During October, these anomalies persist in some years

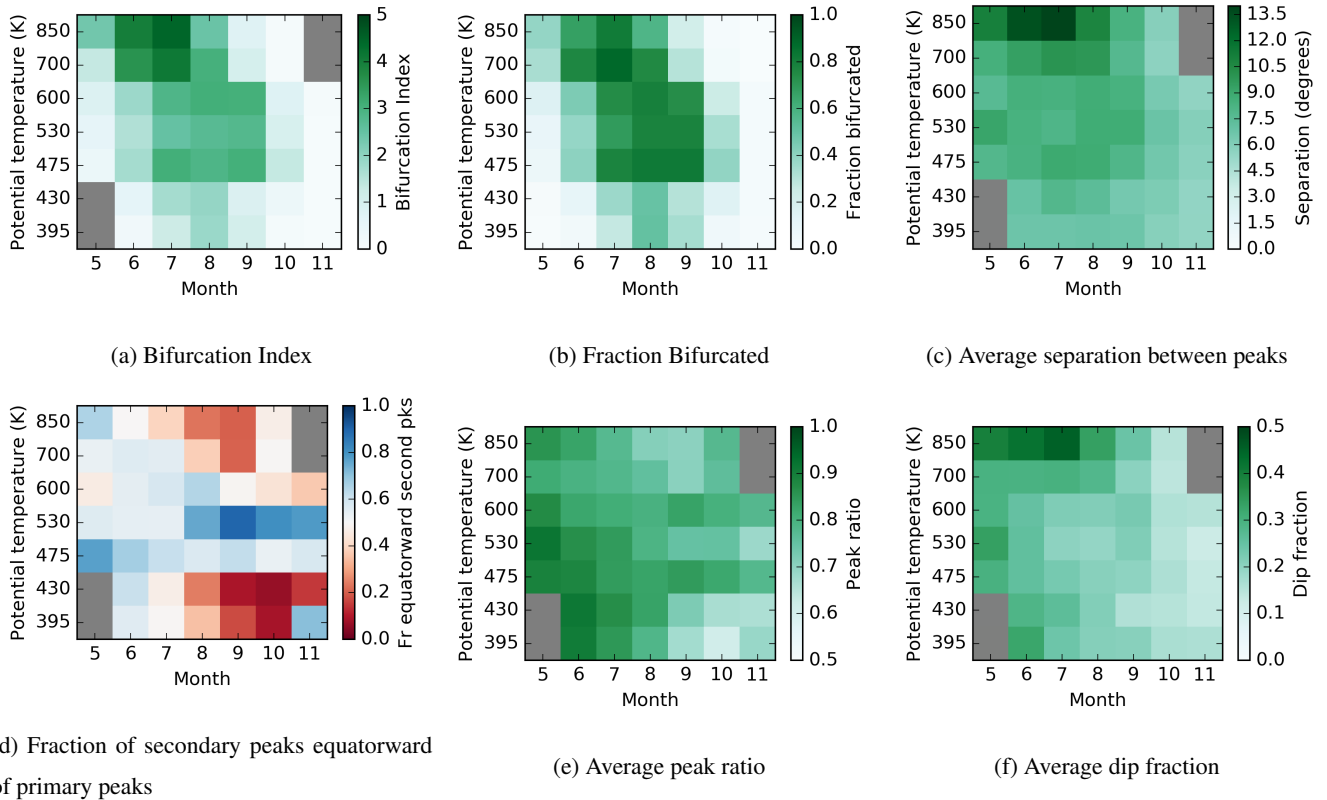


Figure 4. Climatological structure and seasonal evolution of bifurcation metrics derived at ERA-Interim levels between 370K–395K and 850K, 1979–2016. ~~Data is only shown for months~~ Months/levels with less than 1% of bifurcated profiles are shaded in which the climatological vortex is well developed at a given level, identified by an average maximum PV gradient > 0.45 sPVU deg⁻¹ grey.

and are largely confined to 475K to 600K. In November, the single-wall barrier predominates and bifurcation (monthly average BI > 0.75) is only seen in some years two years (1987 at 475K and 530K, and 2015 at 600K).

4 Discussion

4.1 Comparison with CFSR

- 5 Average BI calculated from CFSR shows a very similar structure to that observed in ERA-Interim (Figure 7). Bifurcation generally decreases during the spring, but remains strong at 550K and 650K. The tendency for secondary peaks to occur equatorward of primary peaks is largely restricted to the 550K layer, with 650K and 450K layers displaying similar structure to those at 700K and 430K in ERA-Interim, respectively. The average locations of primary and secondary peaks are similar, with the primary peaks at 550K being most often in the poleward position (-63°) during September (Figure 8). At 650K and
- 10 450K, primary peaks are most often situated at an equatorward location (around -55° to -58°). The occurrence of bifurcation

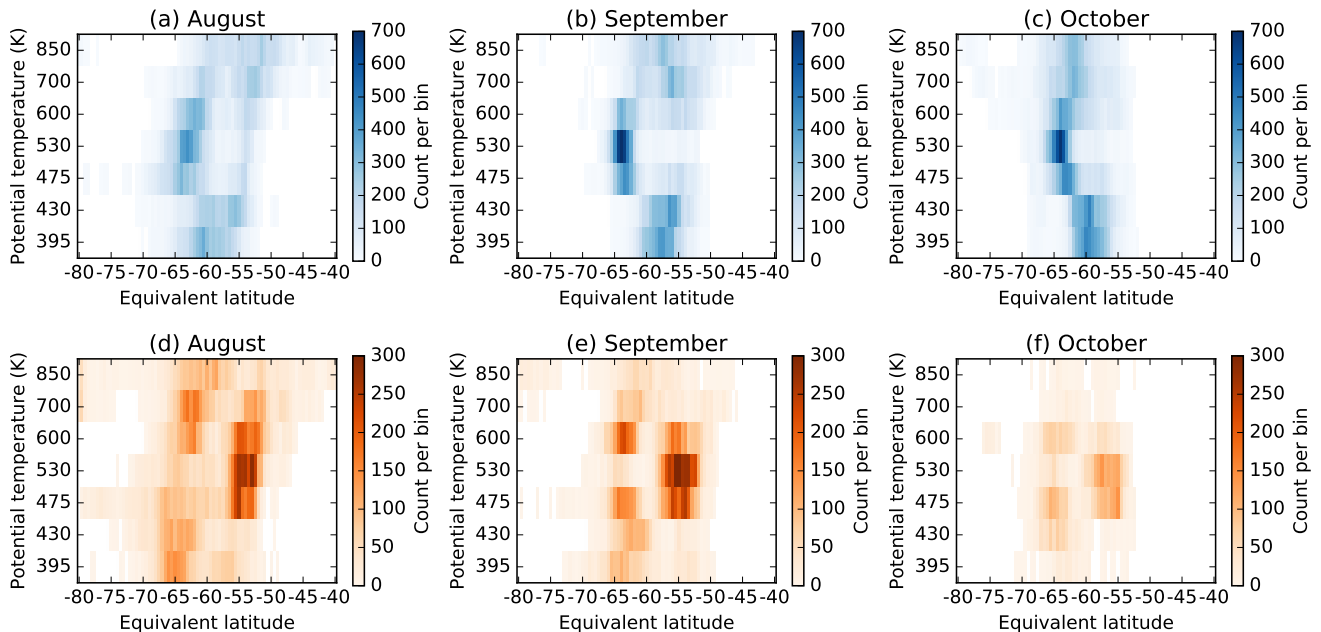


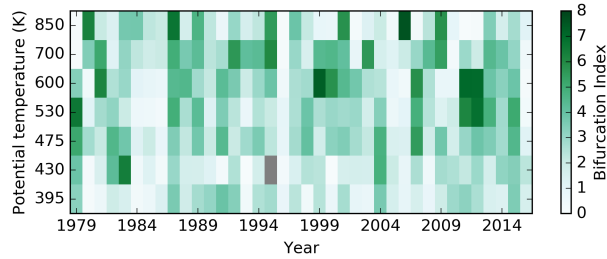
Figure 5. Locations of (a-c) primary and (d-f) secondary peaks in PV gradient at ERA-Interim levels between [370K-395K](#) and 850K, 1979-2016. Peaks are selected using a minimum separation of 5deg and the colour scale shows the number of time steps that peaks occurred in each 0.5deg bin.

in a second reanalyses gives us confidence that the patterns observed are real phenomena and not artefacts of the production of a particular reanalysis data set.

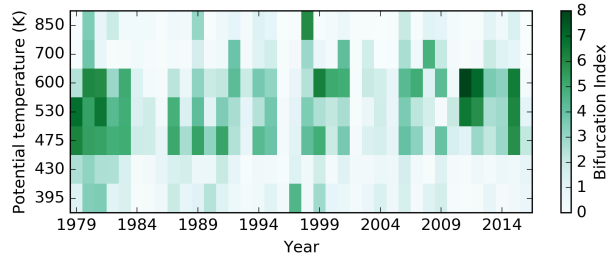
4.2 Impacts of bifurcated PV gradients

The bifurcation of PV gradients across the Southern Hemisphere polar vortex represents a [pause-weakening](#) in the rapid meridional [increase-decrease](#) in PV that occurs across the vortex barrier. Even though PV gradients weaken between the poleward and equatorward peaks, they are still substantially larger than those in the mid-latitudes or the vortex interior. [The To examine the cause of bifurcation in PV gradients, we decomposed PV into its two components, absolute vorticity and static stability \(\$\partial\theta/\partial p\$ \[\$KPa^{-1}\$ \]\), then calculated gradients of these components with respect to EL. Absolute vorticity was calculated from relative vorticity fields downloaded from the ECMWF online archive and latitude at each grid point. Static stability was back-calculated from PV and absolute vorticity at each grid point using the equation for Ertel PV.](#)

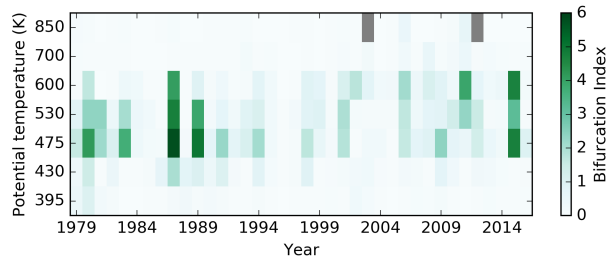
[The gradients of vorticity and static stability at 530K \(Figure 9\) reveal the](#) most rapid decreases in PV occur at the points where relative [vorticity also displays](#) (and absolute) vorticity also display the most rapid decrease - in the transition from the positive vorticity associated with increasing wind speed on the outer flank of the vortex, and to the large negative vorticity associated with decreasing wind speed on the inner flank of the vortex ([see example Figure 9](#)). [In addition, the gradient of static](#)



(a) JulyAugust



(b) September



(c) NovemberOctober

Figure 6. Time series of monthly average BI at ERA-Interim levels between 370K-395K and 850K, 1979-2016. Data is only shown at levels in which Grey colours indicate months with greater than 50% of profiles that do not meet the climatological vortex is well developed in a given month – see Figure 4 caption minimum wind speed and PV gradient criteria.

stability is greater on the inside flank of the vortex. Thus, bifurcation of PV gradients appears to be caused by the separation of two distinct zones of rapidly decreasing relative vorticity. Gradients of absolute vorticity follow closely those in relative vorticity, while the vertical gradient of Θ does not display any obvious bifurcation in concert with stronger gradients of static stability on the inner boundary of the vortex. During periods where the barrier is narrow, the two zones of enhanced vorticity

5 gradient coalesce and only a single peak in PV gradient remains.

To extend this analysis further, we construct latitude-height composites of gradients in each component; for 1 July from five years with strong bifurcation at upper levels (700 and 800K) and for 1 August and 1 September from five years with strong

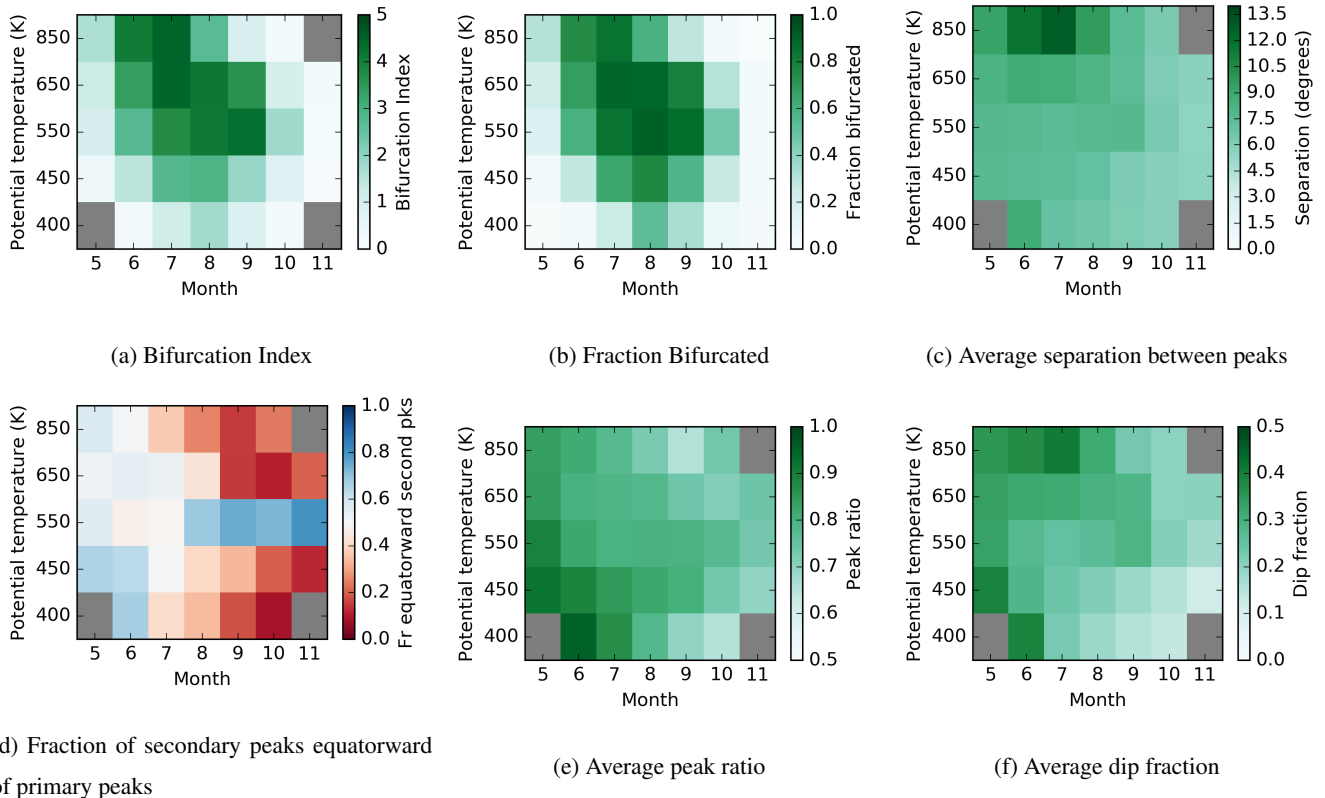


Figure 7. Climatological structure and seasonal evolution of bifurcation metrics at CFSR levels between ~~350K-400K~~ and 850K, 1979-2016. ~~Data are only shown for months in which the climatological vortex is well developed at a given level—see Figure 4 caption. Months/levels with less than 1% of bifurcated profiles are shaded in grey.~~

bifurcation at mid levels (475 to 600K) (Figure 10). The composite analysis reinforces that bifurcation of PV gradients during August and September is associated with elevated vorticity gradients in two locations along with increased static stability gradients at the poleward location. A clear distinction in the location of maximum vorticity gradients is seen during bifurcation at mid-levels during August and September. During years with strong bifurcation at upper levels during July, the location of maximum absolute vorticity and pattern of static stability is less clear, suggesting that the location of bifurcated peaks is more dispersed, and/or the mechanism causing bifurcation at upper levels is more complex.

The weakening of PV gradients within the vortex barrier during periods of bifurcation may increase mixing within the vortex boundary region, while still reducing the transport of material through the barrier as a whole. This could lead to more complex variations of trace gas concentrations across the barrier. With a single (narrower) barrier, there is less efficient mixing of air and steeper gradients in trace gas concentrations within the vortex barrier region would be expected.

Increased PV gradients observed at mid-levels during spring, on the inner flank of the vortex barrier (Figure ??5b), align with the outer limits of regions of enhanced ozone loss (Lee et al., 2001; Bodeker et al., 2002). This provides motivation for

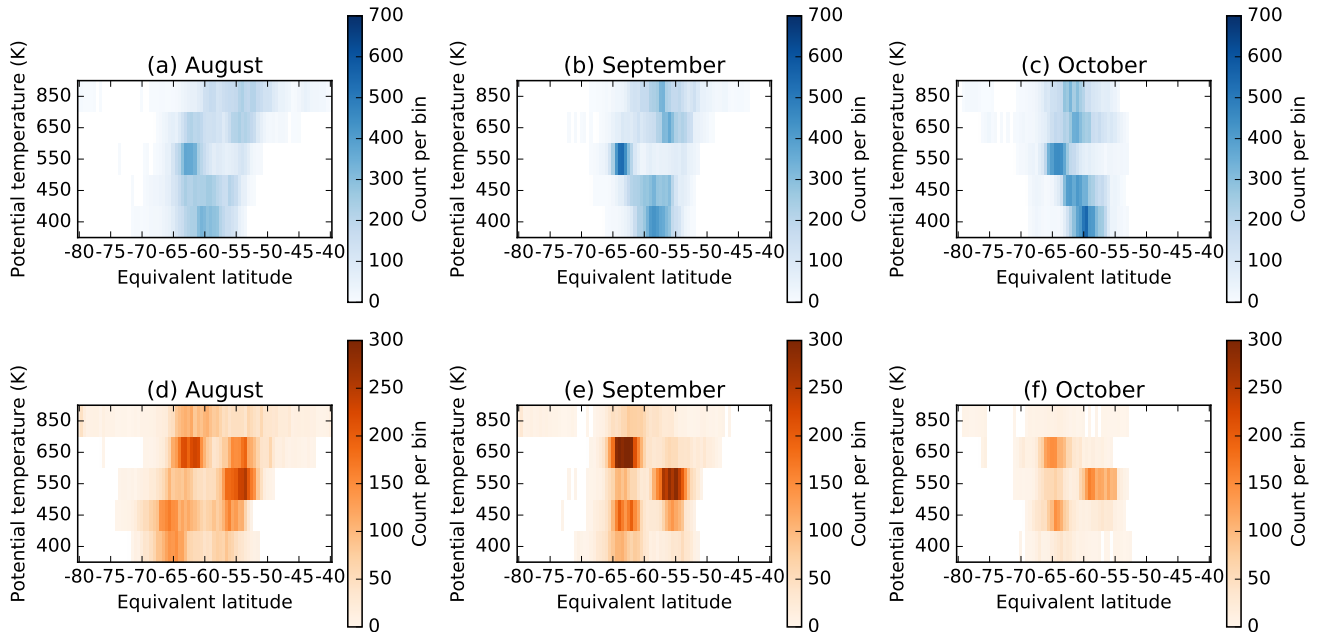


Figure 8. Locations of (a-c) primary and (d-f) secondary peaks in PV gradient at CFSR levels between [350K-400K](#) and 850K, 1979-2016. Peaks are selected using a minimum separation of 5° and the colour scale shows the number of time steps that peaks occurred in each 0.5° bin.

updated analyses of trends in vortex attributes, such as BI, to provide context for recent [reports of](#) trends in ozone concentrations observed during September (e.g. Solomon et al., 2016). [Further work should investigate the dynamical links between ozone loss and PV gradients on the inner boundary of the vortex at mid-levels.](#)

4.3 Redefining a vortex barrier region

- 5 If a single vortex ‘edge’ is defined according to Nash et al. (1996), bifurcation can lead to spurious changes in the location of the vortex boundary region over time. In cases where the PV gradient has two peaks of similar magnitude, the location of the ‘edge’ will flip-flop from one location to the other over the course of a few days, while clearly the vortex has not rapidly changed in size ([Figure 11](#)). This challenges interpretations of the vortex ‘edge’ that define a single location at the maximum PV gradient. By using the bifurcation algorithm described above to detect secondary peaks in the PV gradient, a more realistic
- 10 and robust analysis of the location of vortex barrier is made possible.

The Nash et al. (1996) definition of the vortex boundary region is also challenged by the bifurcated structure. The vortex boundary cannot be simply thought of as the region between the local maximum and local minimum in the second derivative of PV with respect to EL around the location of the primary peak in PV gradient. The presence of secondary peaks in PV gradient

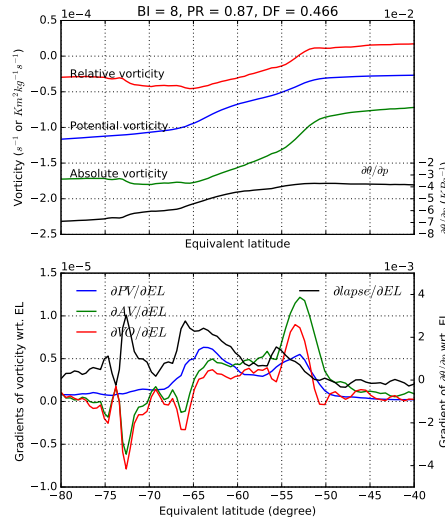


Figure 9. Example meridional profile of (a) (LH axis) gradients of PV with respect to EL ($\partial PV/\partial EL$ ($sPVU deg^{-1}$) and $\partial^2 PV/\partial EL^2$ ($sPVU deg^{-2}$)) and (RH axis) wind speed (ms^{-1}), and (b) (LH axis) absolute and relative vorticity (s^{-1}), PV ($Km^2kg^{-1}s^{-1}$), and (RH axis) vertical gradient of potential temperature (KPa^{-1}), (a) (LH axis) absolute (AV) and relative vorticity (VO) (s^{-1}), PV ($Km^2kg^{-1}s^{-1}$), and (RH axis) static stability (KPa^{-1}), and (b) gradients with respect to EL ($\partial PV/\partial EL$ ($sPVU deg^{-1}$)). All lines are averages at EL calculated from PV. This example is from 530K on 1 September 2007-2011 in ERA-Interim.

inside or outside the primary peak highlights that region of limited mixing is, in fact, much wider than that analysed around only the primary peak.

When the bifurcation is taken into account, the width of the vortex boundary region becomes much larger than that analysed with the Nash et al. (1996) definition (Figure 12). During August and September, a clear separation between inner and outer edges becomes apparent at mid-levels. The inner edge is predominately around -65°, with the outer edge at around -52° to -54°. At times, the outer edge is poleward of -60°, but the inner edge is rarely equatorward of -60°. At lower levels the boundary region is usually confined to a small area around the primary peak at -60°, while at higher levels, the location and width of the boundary region are much more variable. As spring progresses the boundary region coalesces at all levels.

This study suggests there is a need to redefine the location of the vortex barrier as a boundary region in which mixing is reduced below some critical threshold, rather than as a single 'edge'. This definition would demarcate only the inner and outer edges of the vortex boundary region, and would not be dependent on defining a single vortex 'edge' location for the vortex edge. If a single EL or PV value is needed to demarcate the vortex, then the average EL of the boundary region could still be calculated, but this value would be more robust against bifurcation than a single 'edge'. The extension of the Nash et al. (1996) methodology shown here shows promise. Defining threshold values of PV gradient may also be a useful way to define the barrier region, though a formal comparison with other metrics of isentropic mixing (e.g. effective diffusivity, Lyapunov exponents) is warranted. This comparison would allow complementary values of each metric to demarcate the inner and outer edges to be inferred.

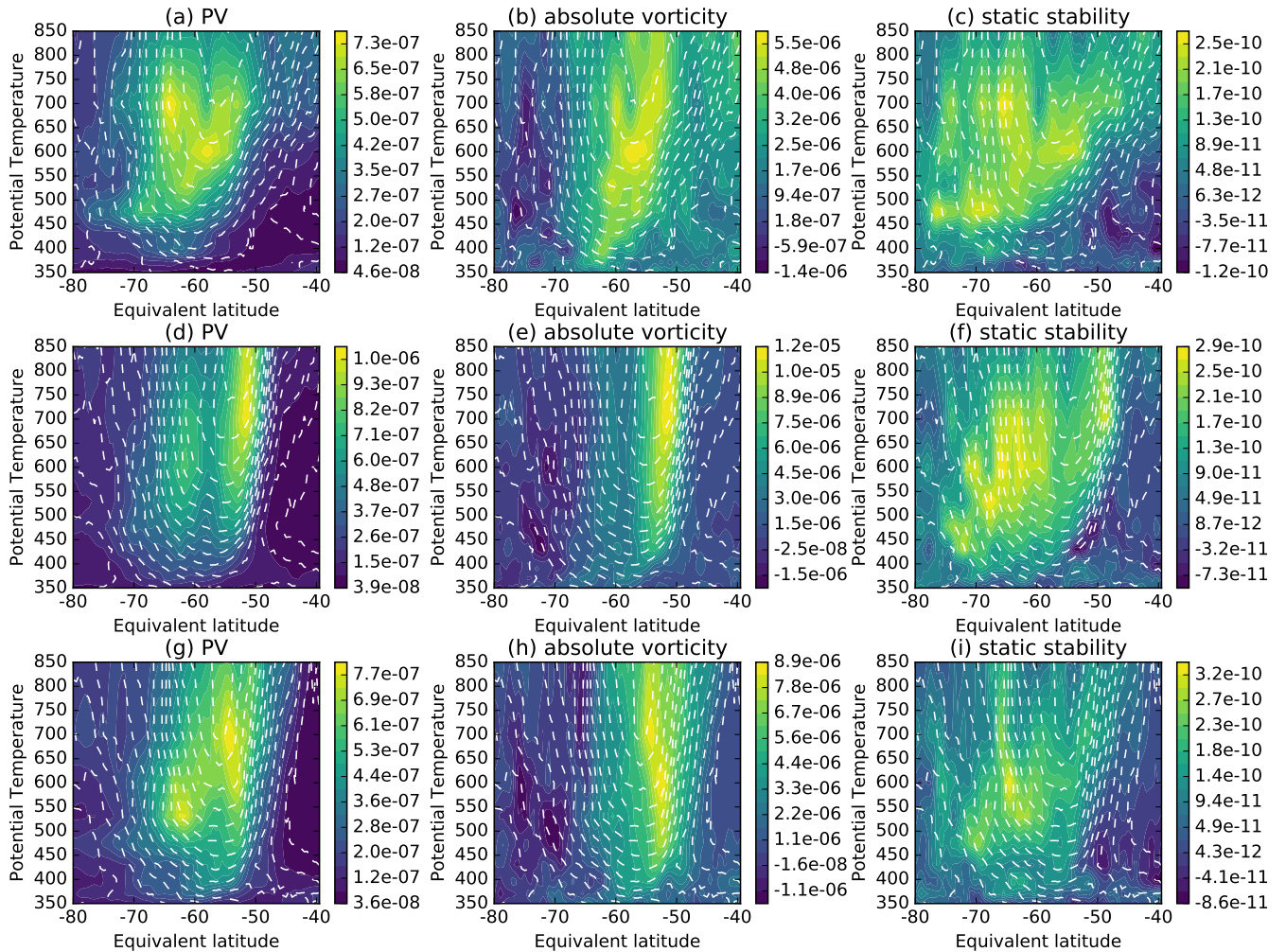


Figure 10. Gradients of PV, absolute vorticity and static stability with respect to EL for composites of years with elevated BI in selected months (a-c) July [1983,1986,1989,1991,2005], (d-f) August [1979,2007,2011,2012,2015] and (h-j) September [1980,1981,2011,2012,2015]. See text for further explanation of method used to select years.

5 Conclusions

The strength of the dynamical isolation of high-latitude air caused by the Southern Hemisphere polar vortex has been analysed using gradients of potential vorticity along equivalent latitude coordinates for ~~nine~~ ~~seven~~ isentropic levels between ~~350K~~ ~~395K~~ and 850K in the ERA-Interim reanalysis for the years 1979-2016. Analyses presented here show that this barrier often displays a bifurcated structure where, rather than a single barrier to meridional mixing, a doubled-walled barrier exists. The bifurcated structure manifests as enhanced gradients of potential vorticity at two distinct equivalent latitudes - usually the inside and outside flanks of the region of highest with enhanced wind speed.

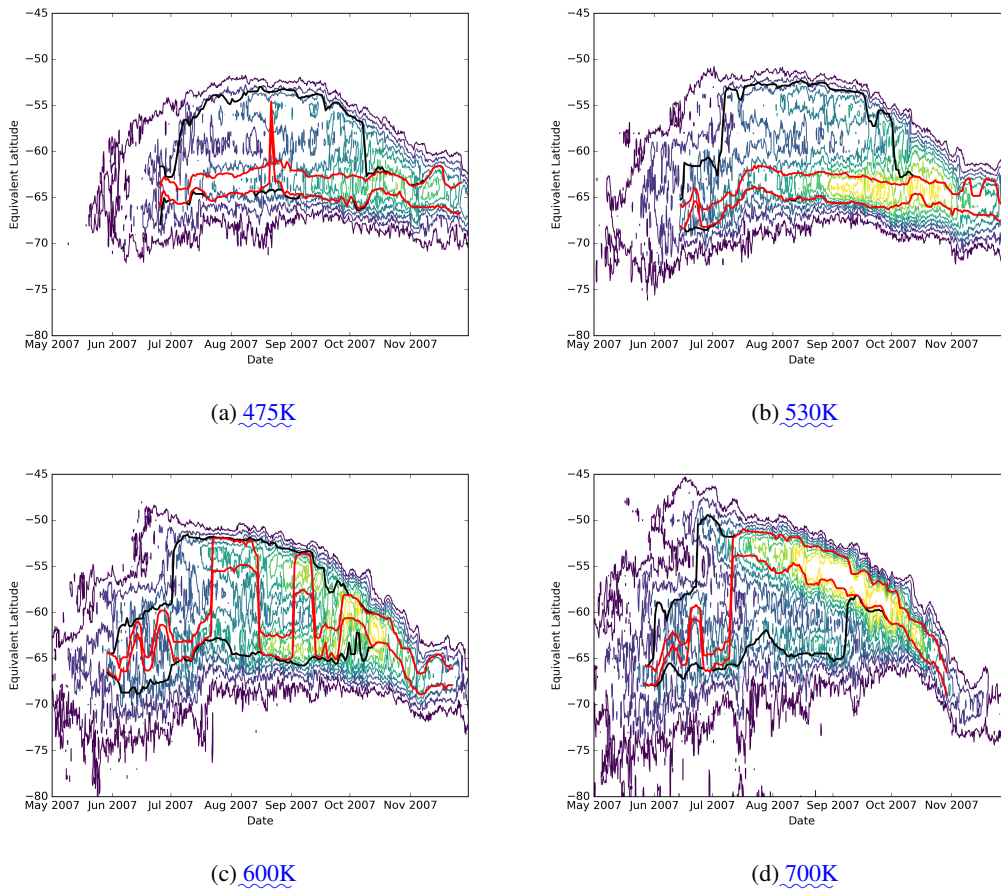


Figure 11. Example showing evolution of PV gradient (coloured contours) and 7-day running average of inner and outer edges diagnosed using (red) the Nash et al. (1996) algorithm or (black) the BI algorithm presented here, during 2007 for four ERA interim heights. Where the black line is not visible, it is in the same position as the red line. Contours of PV gradient are given in 0.15 sPVU steps from 0.3 sPVU to 1.5 sPVU.

Metrics quantifying the bifurcated nature of the vortex barrier have been developed and their variation in space and time has been analysed. While the height-latitude structure differs from year to year, bifurcation appears to be a persistent feature of the vortex barrier region. It was found that at most isentropic levels between 370K-395K and 850K, bifurcation is strongest in winter and reduces dramatically during spring as the barrier becomes more defined. From August onwards, a distinct structure emerges, with stronger bifurcation at mid-levels (475K to 600K) and a mostly single-walled barrier at other levels. During September, peaks in PV gradient show a strong preference for two locations around -63° and -55° and primary peaks at 530K are most often at the poleward location. While the strength of the bifurcation at a given level evolves from month to month and does not always persist through a season, inter-annual variations display coherence across multiple levels in any given month.

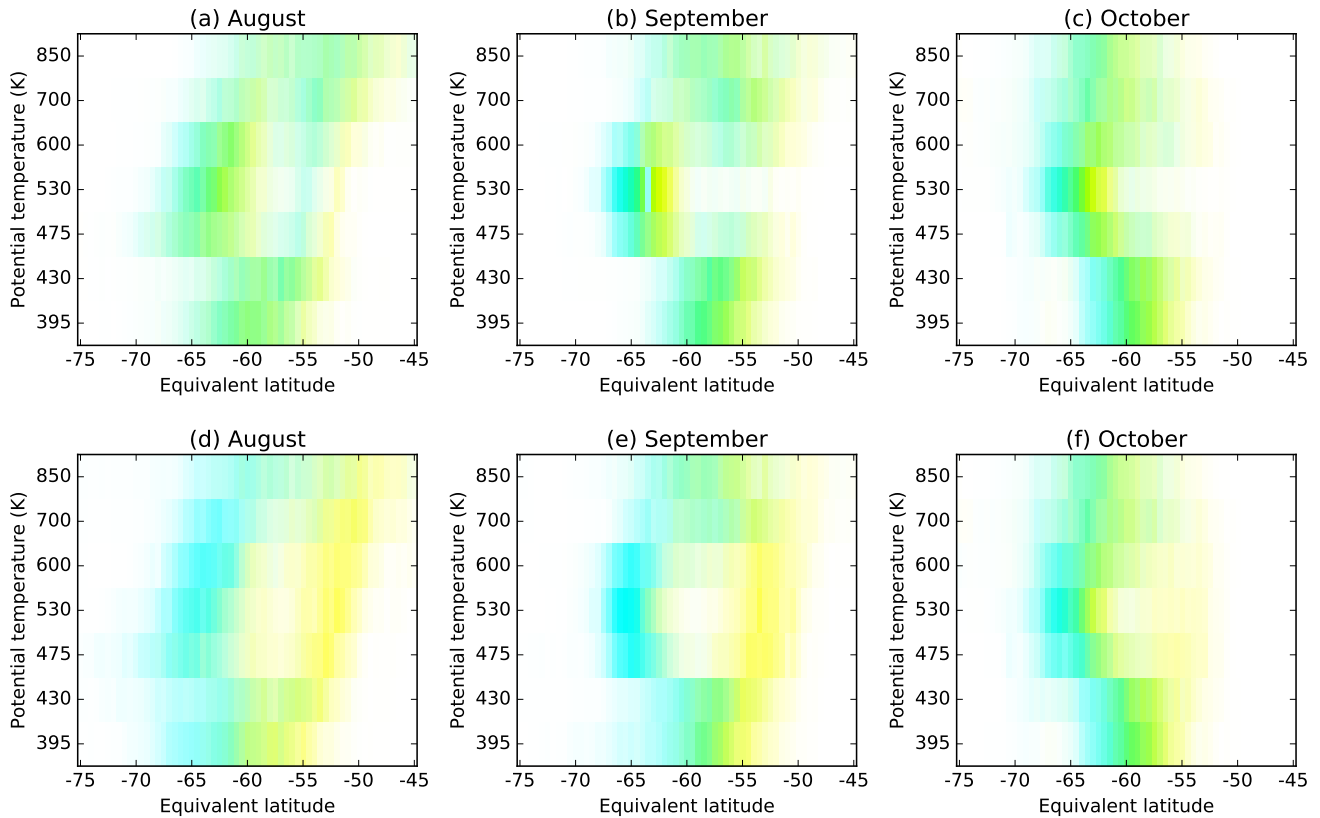


Figure 12. Location of inner (cyan) and outer (yellow) edges of the vortex boundary region at ERA-Interim levels between [370K-395K](#) and 850K, 1979-2016. ~~The vortex boundary region is defined using the criteria of Nash et al. (1996) but also accounts for secondary peaks in PV gradient.~~ defined using (top row) the criteria of Nash et al. (1996) and (bottom row) accounting for secondary peaks in PV gradient using the bifurcation algorithm presented here. The intensity of cyan and yellow represents the frequency of inner and outer boundaries in each 0.5° bin, respectively, with green colours indicating a mix of both inner and outer boundaries at different times. The frequency per bin is scaled with respect to a maximum count of 600 per bin.

Analysis of a second reanalysis, CFSR, shows very similar patterns. The detection of secondary peaks in PV gradient permits a more realistic view of the true region of weak mixing associated with the polar vortex.

The results presented above suggest that improved understanding of cross-vortex mixing requires consideration of the polar vortex not as a single mixing barrier, but as a barrier with internal structure that is likely to manifest as more complex gradients in trace gas concentrations across the vortex boundary region. More work is needed to quantify relationships between PV gradients and other metrics of mixing (effective diffusivity, Lyapunov exponents) as well as identify the interactions between

the structure of PV gradients, ozone and temperature. Analyses of trends in bifurcation should also be pursued to provide context to observed trends in ozone concentrations during springtime.

Data availability. The ERA-Interim data set used in this paper is available from the ECMWF online archives: <http://apps.ecmwf.int/datasets>. The CFSR and CFSv2 data sets are available from <https://rda.ucar.edu/datasets/ds093.0/> and <https://rda.ucar.edu/datasets/ds094.0/>, respectively.

Author contributions. JC developed and performed the analyses, and prepared the manuscript with contributions from all co-authors.

Competing interests. The authors declare that they have no conflict of interest.

Acknowledgements. This research was funded by a Royal Society of New Zealand Marsden Fund research grant titled "The permeability of the Antarctic vortex", contract number BDS1401.

References

- Ajtić, J., Connor, B. J., Lawrence, B. N., Bodeker, G. E., Hoppel, K. W., Rosenfield, J. E., and Heuff, D. N.: Dilution of the Antarctic ozone hole into southern midlatitudes, 1998–2000, *Journal of Geophysical Research*, 109, 1–9, <https://doi.org/10.1029/2003JD004500>, 2004.
- Bodeker, G. E., Struthers, H., and Connor, B. J.: Dynamical containment of Antarctic ozone depletion, *Geophysical Research Letters*, 29, 1098, <https://doi.org/10.1029/2001gl014206>, 2002.
- Butchart, N. and Remsberg, E. E.: The area of the stratospheric polar vortex as a diagnostic for tracer transport on an isentropic surface, *Journal of Atmospheric Sciences*, 43, 1319–1339, [https://doi.org/10.1175/1520-0469\(1986\)043<1319:TAOTSP>2.0.CO;2](https://doi.org/10.1175/1520-0469(1986)043<1319:TAOTSP>2.0.CO;2), 1986.
- Dee, D. P., Uppala, S. M., Simmons, A. J., Berrisford, P., Poli, P., Kobayashi, S., Andrae, U., Balmaseda, M. A., Balsamo, G., Bauer, P., Bechtold, P., Beljaars, A. C. M., van de Berg, L., Bidlot, J., Bormann, N., Delsol, C., Dragani, R., Fuentes, M., Geer, A. J., Haimberger, L., Healy, S. B., Hersbach, H., Hólm, E. V., Isaksen, I., Kållberg, P., Köhler, M., Matricardi, M., McNally, A. P., Monge-Sanz, B. M., Morcrette, J. J., Park, B. K., Peubey, C., de Rosnay, P., Tavolato, C., Thépaut, J. N., and Vitart, F.: The ERA-Interim reanalysis: configuration and performance of the data assimilation system, *Quarterly Journal of the Royal Meteorological Society*, 137, 553–597, <https://doi.org/10.1002/qj.828>, 2011.
- Dunkerton and Delisi: Evolution of Potential Vorticity in the winter Stratosphere of January-February 1979, *Journal of Geophysical Research*, 91, 1986.
- Fujiwara, M., Wright, J. S., Manney, G. L., Gray, L. J., Anstey, J., Birner, T., Davis, S., Gerber, E. P., Harvey, V. L., Hegglin, M. I., Homeyer, C. R., Knox, J. A., Krüger, K., Lambert, A., Long, C. S., Martineau, P., Molod, A., Monge-Sanz, B. M., Santee, M. L., Tegtmeier, S., Chabrilat, S., Tan, D. G. H., Jackson, D. R., Polavarapu, S., Compo, G. P., Dragani, R., Ebisuzaki, W., Harada, Y., Kobayashi, C., McCarty, W., Onogi, K., Pawson, S., Simmons, A., Wargan, K., Whitaker, J. S., and Zou, C.-Z.: Introduction to the SPARC Reanalysis Intercomparison Project (S-RIP) and overview of the reanalysis systems, *Atmospheric Chemistry and Physics*, 17, 1417–1452, <https://doi.org/10.5194/acp-17-1417-2017>, 2017.
- Garny, H., Bodeker, G. E., and Dameris, M.: Trends and variability in stratospheric mixing: 1979–2005, *Atmospheric Chemistry and Physics*, 7, 5611–5624, <https://doi.org/10.5194/acp-7-5611-2007>, 2007.
- Haynes, P. and Shuckburgh, E.: Effective diffusivity as a diagnostic of atmospheric transport: 1. Stratosphere, *Journal of Geophysical Research: Atmospheres*, 105, 22 777–22 794, <https://doi.org/10.1029/2000jd900093>, 2000.
- Hoskins, B., McIntyre, M., and Robertson, A.: On the use and significance of isentropic potential vorticity maps, *Quarterly Journal of the Royal Meteorological Society*, 111, 877–946, <https://doi.org/10.1002/qj.49711147002>, 1985.
- Lait, L.: An alternative form of Potential Vorticity, *Journal of the Atmospheric Sciences*, 51, 1754–1759, [https://doi.org/10.1175/1520-0469\(1994\)051<1754:AAFFPV>2.0.CO;2](https://doi.org/10.1175/1520-0469(1994)051<1754:AAFFPV>2.0.CO;2), 1994.
- Lawrence, Z. D. and Manney, G. L.: Characterizing Stratospheric Polar Vortex Variability With Computer Vision Techniques, *Journal of Geophysical Research: Atmospheres*, 123, 1510–1535, <https://doi.org/10.1002/2017jd027556>, 2018.
- Lee, A., Roscoe, H., Jones, A., Haynes, P., Shuckburgh, E., Morrey, M., and Pumphrey, H.: The impact of the mixing properties within the Antarctic stratospheric vortex on ozone loss in spring, *Journal of Geophysical Research*, 106, 3203–3211, <https://doi.org/10.1029/2000JD900398>, 2001.
- Manney, G. L. and Lawrence, Z. D.: The major stratospheric final warming in 2016: dispersal of vortex air and termination of Arctic chemical ozone loss, *Atmospheric Chemistry and Physics*, 16, 15 371–15 396, <https://doi.org/10.5194/acp-16-15371-2016>, 2016.

- Manney, G. L., Sabutis, J. L., Allen, D. R., Lahoz, W. A., Scaife, A. A., Randall, C. E., Pawson, S., Naujokat, B., and Swinbank, R.: Simulations of Dynamics and Transport during the September 2002 Antarctic Major Warming, *Journal of the Atmospheric Sciences*, 62, 690–707, <https://doi.org/10.1175/JAS-3313.1>, 2005.
- Manney, G. L., Daffer, W. H., Zawodny, J. M., Bernath, P. F., Hoppel, K. W., Walker, K. A., Knosp, B. W., Boone, C., Remsberg, E. E., Santee, M. L., Harvey, V. L., Pawson, S., Jackson, D. R., Deaver, L., McElroy, C. T., McLinden, C. A., Drummond, J. R., Pumphrey, H. C., Lambert, A., Schwartz, M. J., Froidevaux, L., McLeod, S., Takacs, L. L., Suarez, M. J., Trepte, C. R., Cuddy, D. C., Livesey, N. J., Harwood, R. S., and Waters, J. W.: Solar occultation satellite data and derived meteorological products: Sampling issues and comparisons with Aura Microwave Limb Sounder, *Journal of Geophysical Research*, 112, <https://doi.org/10.1029/2007jd008709>, 2007.
- McDonald, A. J. and Smith, M.: A technique to identify vortex air using carbon monoxide observations, *Journal of Geophysical Research: Atmospheres*, 118, 12,719–12,733, <https://doi.org/10.1002/2012jd019257>, 2013.
- Nash, E. R., Newman, P. A., Rosenfield, J. E., and Schoeberl, M. R.: An objective determination of the polar vortex using Ertel’s potential vorticity, *Journal of Geophysical Research: Atmospheres*, 101, 9471–9478, <https://doi.org/10.1029/96jd00066>, 1996.
- Paparella, F., Babiano, A., Basdevant, C., Provenzale, A., and Tanga, P.: A Lagrangian study of the Antarctic polar vortex, *Journal of Geophysical Research: Atmospheres*, 102, 6765–6773, <https://doi.org/10.1029/96jd03377>, 1997.
- Plumb, R. and Ko, M.: Interrelationships between mixing ratios of long-lived stratospheric constituents, *Journal of Geophysical Research*, 97, 10 145–10 156, <https://doi.org/10.1029/92JD00450>, 1992.
- Rummukainen, M., Knudsen, B., and von der Gathen, P.: Dynamical diagnostics of the edges of the polar vortices, *Annales Geophysicae*, 12, 1114–1118, 1994.
- Saha, S., Moorthi, S., Pan, H.-L., Wu, X., Wang, J., Nadiga, S., Tripp, P., Kistler, R., Woollen, J., Behringer, D., Liu, H., Stokes, D., Grumbine, R., Gayno, G., Wang, J., Hou, Y.-T., Chuang, H.-Y., Juang, H.-M. H., Sela, J., Iredell, M., Treadon, R., Kleist, D., Van Delst, P., Keyser, D., Derber, J., Ek, M., Meng, J., Wei, H., Yang, R., Lord, S., Van Den Dool, H., Kumar, A., Wang, W., Long, C., Chelliah, M., Xue, Y., Huang, B., Schemm, J.-K., Ebisuzaki, W., Lin, R., Xie, P., Chen, M., Zhou, S., Higgins, W., Zou, C.-Z., Liu, Q., Chen, Y., Han, Y., Cucurull, L., Reynolds, R. W., Rutledge, G., and Goldberg, M.: The NCEP Climate Forecast System Reanalysis, *Bulletin of the American Meteorological Society*, 91, 1015–1057, <https://doi.org/10.1175/2010bams3001.1>, 2010.
- Saha, S., Moorthi, S., Wu, X., Wang, J., Nadiga, S., Tripp, P., Behringer, D., Hou, Y.-T., Chuang, H.-y., Iredell, M., Ek, M., Meng, J., Yang, R., Mendez, M. P., van den Dool, H., Zhang, Q., Wang, W., Chen, M., and Becker, E.: The NCEP Climate Forecast System Version 2, *Journal of Climate*, 27, 2185–2208, <https://doi.org/10.1175/jcli-d-12-00823.1>, 2014.
- Schoeberl, M. R. and Newman, P. A.: A multiple-level trajectory analysis of vortex filaments, *Journal of Geophysical Research: Atmospheres*, 100, 25 801–25 815, <https://doi.org/10.1029/95JD02414>, 1995.
- Schoeberl, M. R., Lait, L. R., Newman, P. A., and Rosenfield, J. E.: The structure of the polar vortex, *Journal of Geophysical Research: Atmospheres*, 97, 7859–7882, <https://doi.org/10.1029/91JD02168>, 1992.
- Serra, M., Sathe, P., Beron-Vera, F., and Haller, G.: Uncovering the Edge of the Polar Vortex, *Journal of the Atmospheric Sciences*, 74, 3871–3885, <https://doi.org/10.1175/jas-d-17-0052.1>, 2017.
- Smith, M. L. and McDonald, A. J.: A quantitative measure of polar vortex strength using the function M, *Journal of Geophysical Research: Atmospheres*, 119, 5966–5985, <https://doi.org/10.1002/2013jd020572>, 2014.
- Solomon, S.: Stratospheric ozone depletion: a review of concepts and history, *Reviews of Geophysics*, 37, 275–316, <https://doi.org/10.1029/1999RG900008>, 1999.

Solomon, S., Ivy, D. J., Kinnison, D., Mills, M. J., Neely, R. R., and Schmidt, A.: Emergence of healing in the Antarctic ozone layer, *Science*, <https://doi.org/10.1126/science.aae0061>, 2016.

5 Struthers, H., Bodeker, G. E., Austin, J., Bekki, S., Cionni, I., Dameris, M., Giorgetta, M. A., Grewe, V., Lefèvre, F., Lott, F., Manzini, E., Peter, T., Rozanov, E., and Schraner, M.: The simulation of the Antarctic ozone hole by chemistry-climate models, *Atmospheric Chemistry and Physics*, 9, 6363–6376, <https://doi.org/10.5194/acp-9-6363-2009>, 2009.

Waugh, D. W. and Randel, W.: Climatology of Arctic and Antarctic Polar Vortices Using Elliptical Diagnostics, *Journal of the Atmospheric Sciences*, 56, 1999.